International Journal of Geo-Information

MDPI

Article

Urban Vitality Clusters as Activity-Based Diagnostic Units: Spatial Differentiation, Morphological Interpretation, and Planning Translation

Zhenyu Wang [1], Yunfa Wu [1], Fengliang Tang [2] and Weixing Xu [1,*]

[1] School of Architecture and Spatial Planning, Anhui Jianzhu University, No. 292, Ziyun Road, Shushan District, Hefei 230009, China; 15734008806@163.com (Z.W.);
[2] School of Architecture, Tianjin University, Tianjin 300072, China;
* Correspondence: xuwx@tju.edu.cn

Abstract

Urban vitality is often measured within predefined administrative units, blocks, or grids, limiting its translation into planning-oriented spatial diagnosis. This study examines 34 vitality clusters in the Nanjing Metropolitan Area and develops a multi-scale framework linking cluster identification, spatial interpretability, type stratification, morphological differentiation, micro-scale case examination, and planning translation. The identified clusters show substantial correspondence with built-up territories while extending across administrative boundaries in several cases. Five operational area–density groups are distinguished using study-specific thresholds. Their distribution reveals a gradient from high-density cores to medium-density and peripheral low-density clusters, together with an internal pattern of high-vitality cores and lower-vitality edges. After Benjamini–Hochberg correction, 30 of 60 non-redundant variables remained significant, mainly in functional, transport, and morphological dimensions. Micro-scale cases further show the co-occurrence of smaller blocks, continuous frontages, mixed functions, and favorable walking conditions. These findings suggest that vitality-derived clusters can serve as morphologically interpretable, activity-based diagnostic units that complement conventional planning units in stock-based urban regeneration.

Keywords: urban vitality; vitality clusters; activity-based diagnostic units; spatial morphology; urban regeneration; planning translation

Academic Editors: Agnese Pinto, Filippo Gramegna, Saverio Ieva, Floriano Scioscia, Michele Ruta and Wolfgang Kainz

Received: 24 July 2026
Revised: 18 September 2026
Accepted: 24 September 2026
Published: 15 October 2026

Copyright: © 2026 by the authors. Published by MDPI on behalf of the International Society for Photogrammetry and Remote Sensing. Licensee MDPI, Basel, Switzerland. This article is an open access article distributed under the terms and conditions of the Creative Commons Attribution (CC BY) license.

1. Introduction

Urban regeneration has shifted from large-scale incremental development toward the fine-grained governance of existing urban space [1]. Compared with conventional new-area development, stock-based regeneration places greater emphasis on the integrated diagnosis of existing spatial resources, everyday activity demand, public-service provision, transport organization, and spatial quality [2]. The key issue is not only which areas are “active” or “inactive,” but also how to identify the spatial units that truly accommodate human activities and translate them into planning objects that can be analyzed, compared, and intervened in [3]. Traditional planning practice usually relies on administrative districts, subdistricts, communities, parcels, or regular grids to organize spatial analysis [4]. These units are advantageous for statistical management and policy implementation, yet their boundaries often do not fully correspond to actual activity linkages, functional coupling, and the intensity of spatial use [5].

In recent years, urban vitality research has developed rapidly with the support of multi-source urban big data and machine learning methods [6]. Location-based service data, mobile-phone signaling data, points of interest (POIs), road networks, nighttime lights, street-view images, and remote-sensing images have enabled researchers to identify urban activity intensity, spatial distribution, temporal fluctuation, and influencing factors with greater precision [7–10]. However, existing studies often treat urban vitality as an indicator value assigned to a certain spatial unit, and their outputs are mainly vitality distributions, hot-spot identification, or rankings of influencing factors [11–13]. Such results can answer where vitality is high and which factors matter, but they remain insufficient for addressing whether vitality space can serve as a planning unit, what morphological differences exist among different vitality spaces, and how vitality results can be translated into regeneration strategies [14].

Urban vitality clusters provide a new entry point for this transition. Unlike administrative units, block units, or regular grids, vitality clusters are not predefined management or computational boundaries [4]. Rather, they are spatial concentrations derived from the aggregated distribution of urban activity intensity together with spatial proximity, functional supply, and built-environment conditions [15]. In this sense, this study aims to explore whether clustering based on vitality can be regarded as an activity-based spatial layer for diagnosing urban renewal. Their potential value lies in combining a data-driven basis of identification with the spatial continuity, agglomeration, and functional relationships required for planning interpretation. Vitality clusters may therefore serve as intermediary analytical units connecting urban big-data analysis with the diagnosis of regeneration areas [16].

On this basis, this study takes urban vitality clusters in the Nanjing Metropolitan Area as its research object and examines how vitality-derived spatial clusters can be translated from analytical outputs into morphologically interpretable units for urban-regeneration diagnosis. The study addresses three questions. First, to what extent do the identified vitality clusters exhibit spatial and structural interpretability as analytical units? Second, what hierarchical structures, internal vitality organization, and multi-dimensional morphological differences are exhibited by different types of vitality clusters? Third, how can cluster-level characteristics be further interpreted through micro-scale cases and translated into potential implications for urban regeneration and spatial governance?

The overall research structure is illustrated in Figure 1. The central contribution of this study is a shift in the unit of analysis: from treating urban vitality as an attribute measured within predefined administrative units, blocks, or grids to treating vitality-derived clusters as activity-informed spatial objects that can be morphologically interpreted for regeneration diagnosis. This shift is methodologically important for stock-based urban regeneration because predefined units may fragment continuous activity concentrations or aggregate internally heterogeneous activity conditions, whereas regeneration diagnosis requires spatial objects whose boundaries and internal organization correspond more closely to observed patterns of urban use. On this basis, the study links cluster identification with spatial-interpretability assessment, type stratification, multi-dimensional morphological analysis, and micro-scale case examination. In practical terms, the resulting clusters are not intended to replace statutory planning units but to provide a complementary activity-based diagnostic layer for identifying cross-boundary spatial problems and informing differentiated regeneration strategies.

https://doi.org/10.3390/ijgi15100469

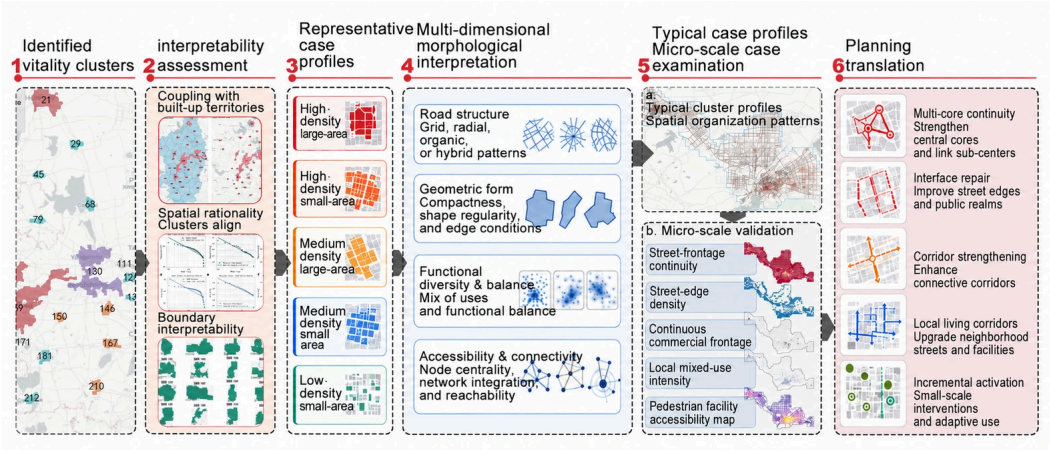


Figure 1. Research framework.

2. Literature Review

2.1. Measuring Urban Vitality: From Observing Street Life to Urban Big-Data Analytics

Urban vitality has long been an important topic in urban studies, urban and rural planning, and urban design [17]. Its early conceptual development was closely associated with observational studies of everyday urban life and the relationship between spatial form and human activity [18–20]. Jacobs (1961) linked lively urban environments to mixed primary uses, short blocks, buildings of different ages, and sufficient concentrations of people, establishing diversity and everyday street activity as central conditions of urban vitality [21]. Gehl (2003 further emphasized the relationship between the quality of spaces between buildings and necessary, optional, and social activities, highlighting the human-scale conditions that encourage people to stay and interact in public space [22]. Montgomery (2007 subsequently connected urban vitality with the interplay among activity, diversity, transaction, urban form, and street life [23]. Together, these foundational studies established a people-centered understanding of vitality in which urban space is evaluated not simply by its physical form but by the activities and interactions that it accommodates [24].

With the development of urban sensing technologies and spatial big data, the measurement of urban vitality has gradually shifted from empirical observation and small-scale surveys to large-scale, high-resolution, multi-source quantitative analysis [25]. Location-based service data, mobile-phone signaling data, POIs, social-media check-ins, nighttime lights, transit smart-card records, taxi trajectories, street-view images, and remote-sensing images have been widely used to characterize activity intensity, spatiotemporal distribution, functional agglomeration, and spatial attractiveness [6,26–28].

Overall, existing studies have substantially improved the precision, spatial resolution, and analytical scope of urban vitality measurement. However, two limitations remain relevant to planning-oriented applications. First, vitality is commonly represented as an attribute attached to predefined administrative units, blocks, or grids, while the spatial continuity of observed activity is less frequently treated as an object of analysis in its own right. Second, most studies focus on measuring vitality patterns or explaining their determinants, leaving a gap between vitality measurement and the delineation of spatial units that can subsequently be interpreted in morphological and planning terms. This gap shifts the question from how vitality is measured to how vitality-derived spatial patterns can be organized into meaningful analytical units, which forms the focus of the study.

2.2. Constructing Spatial Units in Urban Research: Administrative Units, Functional Areas, and Activity Spaces

The delineation of spatial units is a fundamental issue in urban research [29]. Traditional urban planning and spatial analysis usually rely on predefined spatial units such as administrative districts, subdistricts, communities, parcels, census units, blocks, traffic analysis zones, and regular grids. These units have clear significance for management, statistics, and policy implementation, but their boundaries are often determined by institutions, property rights, or computational convenience and cannot fully correspond to actual human activities and spatial-use relationships [30,31].

To overcome the limitations of predefined boundaries, recent urban research has increasingly turned toward functional, behavioral, and relational approaches to spatial-unit construction [32]. Studies of urban functional areas use POIs, land use, remote-sensing images, taxi trajectories, transit smart-card records, and mobile-phone signaling data to identify urban functional structures [33,34]. Activity-space research, in contrast, interprets urban space from everyday behaviors such as commuting, consumption, leisure, public-service use, and social interaction [35]. Importantly, activity spaces and vitality clusters refer to different spatial concepts. Activity spaces are generally individual- or group-centered and describe the geographical extent of actual activities or mobility, whereas vitality clusters are place-centered aggregations derived from the spatial concentration and continuity of urban activity intensity. Therefore, the vitality clusters examined in this study should not be understood as individual activity spaces, but as activity-informed spatial units derived from aggregated urban vitality patterns. Data-driven delineation does not eliminate the modifiable areal unit problem (MAUP) or geographic-context uncertainty; vitality clusters should therefore be understood as an activity-informed analytical layer rather than a scale-free representation of urban activity.

Urban vitality clusters are neither administrative management units nor physical territories delineated purely by material form. Instead, they are activity-based spatial units identified through the joint effects of human activity intensity, spatial proximity, functional supply, and built-environment support [2]. Activity-based planning units do not deny the value of administrative units or physical territories; rather, they provide another explanatory layer [36]. Administrative units answer "who governs," physical territories answer "how space is built," and activity-based units answer "how human activities are organized and how they can be intervened in."

However, delineating an activity-informed spatial unit is only the first step toward planning application. For such units to become useful for urban-regeneration diagnosis, their internal road structure, spatial form, functional organization, accessibility, and street-level conditions must also be interpretable.

2.3. Morphological Interpretation and Planning Translation of Vitality Space

If activity-based spatial units are to enter planning practice, they cannot remain merely maps of urban vitality distribution; they must also be morphologically interpreted [9]. Urban-morphology research has long focused on the relationships among road networks, block structure, parcel organization, building form, functional layout, and public space, providing an important basis for understanding how spatial structure influences urban activity [37].

The formation of urban vitality depends on multi-dimensional spatial conditions. Road networks determine the organization of flows and accessible routes [38]; block scale affects walking convenience and spatial permeability [1]; building frontages determine the accessibility of ground floors and the continuity of streets [39]; functional mix affects the superposition of activities across different times and user groups [40]; and

public transport and slow-mobility systems determine whether activities can diffuse over wider areas.

Accordingly, the morphological interpretation in this study is organized around five complementary dimensions rather than individual indicators in isolation. Road-structure measures characterize the density and directional organization of the movement network; geometric-form measures describe compactness and boundary complexity; distribution and agglomeration measures capture whether activity-supporting space is concentrated, displaced, or axially organized; accessibility and connectivity measures describe the continuity and topological integration of the road network; and functional-structure measures characterize the diversity and balance of urban functions. Together, these dimensions correspond to the study's central question of how vitality-derived clusters differ in their spatial organization and whether such differences can be meaningfully interpreted for regeneration diagnosis.

Taken together, the three strands of literature reviewed above reveal a sequential gap between vitality measurement, spatial-unit construction, and planning-oriented morphological interpretation. Big-data studies have substantially improved the observation of urban activity, while functional- and activity-space studies have challenged the reliance on predefined spatial boundaries. Urban-morphology research, in turn, provides the conceptual basis for interpreting how roads, spatial form, accessibility, functions, and street environments differentiate urban spaces. Accordingly, this study links spatial-unit interpretation, morphological differentiation, micro-scale case examination, and potential planning translation. The identified clusters represent aggregated activity patterns over the observation period rather than time-varying cluster boundaries.

3. Materials and Methods

3.1. Study Area and Data Basis

This study takes the Nanjing Metropolitan Area as the empirical research area. The Nanjing Metropolitan Area includes Nanjing and several surrounding cities and is an important cross-administrative metropolitan functional region in the Yangtze River Delta, as shown in Figure 2. It contains high-intensity metropolitan cores such as the main urban area of Nanjing, as well as city nodes of different levels, including Zhenjiang, Yangzhou, Ma'anshan, Wuhu, Chuzhou, Huai'an, and Xuancheng. This regional structure provides typical samples for identifying vitality clusters of different scales, densities, and functional structures [41].

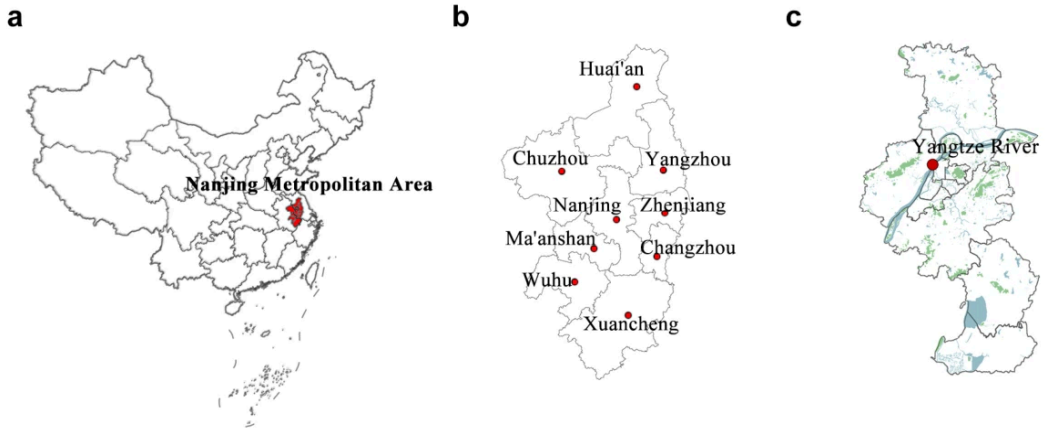


Figure 2. Location of the Nanjing Metropolitan Area.

Based on the Urban Information Box (UIB) framework established in our previous

study [14], the present analysis uses a regular 500 m × 500 m square grid as the basic spatial data unit. Multi-source point, line, polygon, and raster data were aggregated or spatially joined to the corresponding UIB cells, thereby forming a unified spatial–attribute database for subsequent analysis. The scale-selection procedure and detailed construction of the UIB are described in our previous study. This study organizes human activity, POIs, road networks, building morphology, land use, public transport, nighttime lights, population, and economic data into basic spatial units. The human-activity data used to characterize vitality were collected from Baidu heatmaps on 18 May 2022 (weekday) and 22 May 2022 (weekend), with hourly observations covering 24 h on each day. For each hourly observation, UIB-level vitality was first calculated as the arithmetic mean of the Baidu heatmap point values falling within each UIB. Principal component analysis (PCA) was then conducted separately for the 24 hourly weekday and weekend observations to derive temporal weights. The corresponding weighted combinations were used to calculate weekday and weekend static vitality, while the composite static vitality used in the subsequent analysis integrated all 48 hourly observations using the corresponding PCA-derived weights. Detailed temporal weights are provided in Supplementary Table S20c.

All vector-based metric calculations, including cluster area, road length, geometric distance, and density measures, were performed in WGS 84/UTM Zone 50N (EPSG:32650). All geometry-derived indicators were rechecked under this common projected coordinate system to ensure consistency in spatial measurement. Building on the UIB-based multi-source data framework developed in our previous studies [14,42], the present study shifts the analytical focus from basic-unit vitality measurement and temporal transfer to the delineation and interpretation of spatially continuous vitality clusters at the metropolitan scale.

For spatial harmonization, the Baidu heatmap data were represented at a 100 m resolution, whereas all other raster datasets were standardized to a 500 m analytical resolution. Dataset years are reported in Table 1, and the activity data retain an hourly temporal resolution, while the remaining spatial datasets are treated as contextual layers for the corresponding study period. Because the heatmap-derived vitality values exhibited a long-tailed distribution, the resulting vitality measure was log-transformed before subsequent analysis. UIBs with fewer than 16 non-zero vitality observations across the 48 hourly records were excluded from the valid activity sample. For each vitality cluster c, mean cluster vitality was calculated as the arithmetic mean of its UIB-level vitality values, while within-cluster variability was represented by the standard deviation of these values. The maximum vitality corresponds to the highest UIB-level vitality value within each cluster.

Table 1. Data sources and descriptions.

Data Name	Data Source	Reference	Data Type	Purpose
POIs	Amap Developer Platform	2022	Point data	Represents urban functions and service facilities.
Classified road network	OpenStreetMap	2022	Line data	Used for road-structure, accessibility, and connectivity analysis.
Building vector data	Baidu Maps Developer Platform	2022	Polygon data	Represents building morphology, development intensity,

Data Name	Data Source	Reference	Data Type	Purpose
				and spatial structure.
GDP	Gridded GDP data	2022	Raster data	Reflects the spatial distribution of economic activity.
Land-cover data	ESA WorldCover	2021	Raster data	Represents land cover and ecological background.
Digital elevation, NDVI, and NPP	Google Earth Engine	2022	Raster data	Represents topography and ecological environment.
Nighttime-light data	National Earth System Science Data Center	2022	Raster data	Represents nighttime activity and economic intensity.
Resident population data	WorldPop	2022	Raster data	Represents the spatial distribution of population.
Heatmap and social-media data	Baidu Maps Developer Platform and Sina Weibo	18 May and 22 May 2022 (A total of 48 h)	Point/raster data	Provides auxiliary representation of human activity and online attention.

Note: Raster datasets were harmonized to a 500 m analytical resolution, except for the Baidu heatmap data, which were represented at 100 m resolution.

3.2. Methods for Identification of Urban Vitality Clusters

Urban vitality clusters were identified using the Urban Information Box (UIB) as the basic spatial data unit. This study used a 500 m × 500 m UIB grid; the construction and scale determination of the UIB have been described in detail in our previous study [14] and are therefore not repeated here. In the present study, multi-source urban variables were harmonized within the UIB framework and standardized before model input. Following the preceding feature-screening procedure, 13 retained variables were used as model inputs. These comprised the comprehensive urban morphology factor (Mor_PCA), impervious surface ratio (IMPR), walkability score (WS), car accessibility (DTA), comprehensive public transport factor (Bus_PCA), POI Shannon diversity index (POISHDI3), POI density (POIKDE), employment and office facilities (E2PS), cultural and entertainment facilities (C2ES), residential service facilities (RESS), educational facilities (ERS), public transport facilities (APTSS), and nighttime light intensity (NLM). Among them, Mor_PCA and Bus_PCA are composite variables derived through principal component analysis to reduce collinearity among their constituent indicators. The complete definitions of the candidate variables are provided in Supplementary Table S15 , while the final 13 model inputs are listed in Supplementary Table S20. The 13 retained variables served as explanatory model inputs, whereas the UIB-level vitality measure derived from the Baidu heatmap data, as defined in Section 3.1, was used as the prediction target.

Cluster identification employed a spatial representation-learning network based on bidirectional multi-head self-attention. Rather than processing each UIB independently, the model jointly represented the attribute characteristics of each focal UIB and its surrounding spatial context. Specifically, each focal unit was combined with its 28 nearest neighbouring UIBs based on centroid distance, forming a spatial sequence of 29 units. The network compressed the resulting spatial-attribute information into a latent repre-

sentation that preserved both attribute similarity and local spatial dependence. The latent representation was learned under a joint prediction–reconstruction objective, with both terms evaluated using mean squared error.

The learned representations were then clustered using a Gaussian mixture model (GMM), followed by land-cover-based semantic correction and neighbourhood-based spatial smoothing to reduce geographically implausible classifications and isolated patches. Because the cell-based classification could leave short spatial discontinuities and fragmented patches among adjacent UIBs, a two-stage buffer-based consolidation was subsequently applied as a spatial post-processing procedure. The first stage used a 1500 m outward buffer followed by a 1000 m inward contraction to reconnect nearby fragmented patches, after which the result was rasterized at a 500 m resolution and isolated fragments smaller than 5000 m^2 were removed. A second, finer-scale consolidation used a 1000 m outward buffer followed by an 800 m inward contraction, with fragments smaller than 10,000 m^2 removed. The asymmetric outward–inward operations intentionally retained limited spatial connections formed during consolidation rather than restoring the exact pre-buffer geometry. These procedures produced 253 initial candidate clusters. To retain spatial units with sufficient spatial extent and population support, candidates with an area smaller than 3 km^2 or a population below 50,000 were excluded, resulting in 34 final vitality clusters across the Nanjing Metropolitan Area.

The final 34 clusters should therefore be understood as operational spatial units produced through a sequential workflow of representation learning, GMM-based probabilistic partitioning, spatial correction and smoothing, two-stage spatial consolidation, and area–population screening, rather than as direct outputs of the representation-learning network alone.

3.3. Operational Area–Density Grouping of Vitality Clusters

To facilitate comparative analysis, the 34 vitality clusters were stratified by area and population density using study-specific operational thresholds. These groups are operational area–density categories used for comparative analysis, while morphological indicators are, see Table 2 introduced subsequently to examine inter-group spatial differentiation; the thresholds are therefore study-specific rather than universal classification standards. An area threshold of 100 km^2 and population-density thresholds of 1500 and 3000 persons/km^2 were adopted to distinguish larger and smaller clusters and low-, medium-, and high-density conditions, respectively. The selected cutoffs fall within local gaps in the ordered sample distributions, and their sensitivity to alternative area and density thresholds is evaluated in Supplementary Table S16. The sensitivity analysis showed that the operational grouping was comparatively stable under moderate changes in the area and density thresholds, although larger changes in the density thresholds produced greater reassignment. Under the most restrictive alternative specification, 13 of the 34 clusters changed category, corresponding to 61.8% agreement with the baseline grouping, and several alternative specifications produced singleton groups.

Table 2. Operational area–density grouping of vitality clusters.

Type ID	Type Name	Area Range	Population-Density Range
1	High-density large-area	≥100 km^2	≥3000 persons/km^2
2	High-density small-area	<100 km^2	≥3000 persons/km^2
3	Medium-density large-area	≥100 km^2	1500–3000 persons/km^2
4	Medium-density small-area	<100 km^2	1500–3000 persons/km^2
5	Low-density large-area	≥100 km^2	<1500 persons/km^2

Type ID	Type Name	Area Range	Population-Density Range
6	Low-density small-area	<100 km^2	<1500 persons/km^2

3.4. Indicator System for Morphology and Function

To interpret the spatial organization of the identified vitality clusters, this study constructs a morphology-oriented indicator system covering five complementary dimensions: road structure, geometric form, distribution and agglomeration, accessibility and connectivity, and functional structure. The indicators were selected for their ability to represent distinct but complementary properties of cluster morphology, see Table 3 and network organization, rather than for predictive modeling. Together, they allow the identified clusters to be compared in terms of network support, spatial compactness, core organization, internal connectivity, and functional complexity. The full indicators and complete calculation results for the 34 clusters are provided in the Supplementary M aterials.

For the accessibility and connectivity analysis, the road network within each cluster was represented as a graph in which road intersections and topological endpoints were treated as nodes, and road segments connecting adjacent nodes were treated as edges. Random-walk average step length is expressed as the number of graph steps; node coverage is a proportion; the number of connected subgraphs is a count; and average degree and graph density are dimensionless topological measures.

Table 3. Indicator system for morphology and function.

Dimension	Core Indicators	What They Capture	Analytical Role in This Study
Road structure	Total road length, number of road segments, average segment length, road density, dominant-direction ratio, weighted directional standard deviation	Network extent, density and directional organization	How road-network extent, density, and directional organization differ among cluster profiles
Geometric form	Compactness, fractal dimension, boundary complexity	Compactness, irregularity and boundary fragmentation	Whether clusters differ in spatial compactness and boundary organization
Distribution and agglomeration	Centrality, hollowness, dominant-direction angle, distribution type	Concentration, displacement and axial organization	Whether clusters are monocentric, dispersed or corridor-oriented
Accessibility and connectivity	Random-walk average step length, node coverage, number of connected subgraphs, average degree, graph density	Network continuity and topological integration	Whether internal road networks provide continuous spatial linkage
Functional structure	Functional mix, functional balance, core-area functional proportion, average functional distance	Diversity, balance and functional concentration	How functional organization differs among cluster types

3.5. Inter-Group Difference Tests and Micro-Scale Case Examination

To explore inter-group differences across multiple urban dimensions, 60 non-redundant variables were examined using one-way ANOVA or Kruskal–Wallis tests.

Normality (Shapiro–Wilk) and homogeneity of variance (median-centered Levene) were assessed for groups with at least three observations; ANOVA was used when the assessable groups satisfied both assumptions ($p > 0.05$), and Kruskal–Wallis otherwise. Given the small and uneven group sizes (n = 3, 5, 2, 18, and 6), the analyses were treated as exploratory. Multiple testing was controlled using the Benjamini–Hochberg false discovery rate (FDR), with η^2 and ε^2 reported as effect sizes. FDR-significant variables were further examined using Tukey HSD or Dunn tests with Holm adjustment, and all variables were additionally re-tested using Kruskal–Wallis as a robustness check. Spatial dependence was assessed using global Moran's I based on a symmetric four-nearest-neighbour weight matrix, with significance evaluated by 999 permutations and FDR correction. Full statistical results are reported in Supplementary Tables S13 and S17–S19 [43,44].

To further examine how cluster-level morphological differences can be interpreted at the urban-design scale, five representative clusters (#21, #146, #111, #123, and #45) were purposively selected for case-based examination. The selection followed two criteria: coverage of all five empirically observed cluster groups and representation of contrasting morphological configurations identified in the preceding cluster-level analysis. The cases serve as illustrative examples. The micro-scale examination focuses on block scale, street-frontage continuity, street-edge density, continuous commercial frontage, local mixed-use intensity, and walkability to assess whether the cluster-level differences remain interpretable at finer spatial scales.

Walkability was represented by a POI-based road-service score (WS) adapted from the Walk Score approach [45]. Nearby facilities were assigned category-specific weights and distance-decay coefficients based on Euclidean distance within a maximum search radius of 2400 m, with higher weights given to daily commercial and dining facilities. The resulting road-level scores were robustly normalized using the 2nd–98th percentile range to obtain $ws_{norm} \in [0,1]$, and cluster-level indicators were summarized using road-length-weighted statistics. Segments at or above the metropolitan-wide 80th and 90th percentiles of WS were defined as ≥P80 WS segments and ≥P90 WS segments, respectively.

4. Results

4.1. Type Structure and Spatial Hierarchy of Vitality Clusters

Based on the operational area and population-density thresholds, the 34 vitality clusters in the Nanjing Metropolitan Area are classified into five empirical cluster types for comparative analysis: High-density large-area, High-density small-area, Medium-density large-area, Medium-density small-area, and Low-density small-area. The low-density expanded type appears as a theoretical category but is not observed in the identification results, indicating that the formation of vitality clusters generally requires a certain basis of population density, activity intensity, spatial continuity, and functional support.

Cluster area is an output of the identification procedure under spatial-continuity and smoothing constraints rather than a predefined input. Large clusters represented by #189 and #130 show that actual urban vitality space may form continuous cross-administrative agglomerations along transport corridors, functional linkages, and contiguous urbanized areas. This phenomenon indicates that vitality clusters should not be understood simply as fixed-scale block units, but as multi-scalar spatial units jointly generated by activity linkages and the built environment.

Figure 3 shows that most vitality clusters are concentrated within the ranges of 50–100 km^2 and 2000–3000 persons/km^2, displaying the dominant characteristics of

"medium density–small scale." This indicates that vitality space in the Nanjing Metropolitan Area is not entirely dominated by a super-large metropolitan core, but is jointly constituted by many medium-density and relatively compact urban activity units. Large clusters that deviate from this concentrated interval, such as #130 and #189, reflect stronger regional agglomeration, functional integration, and cross-city radiation.

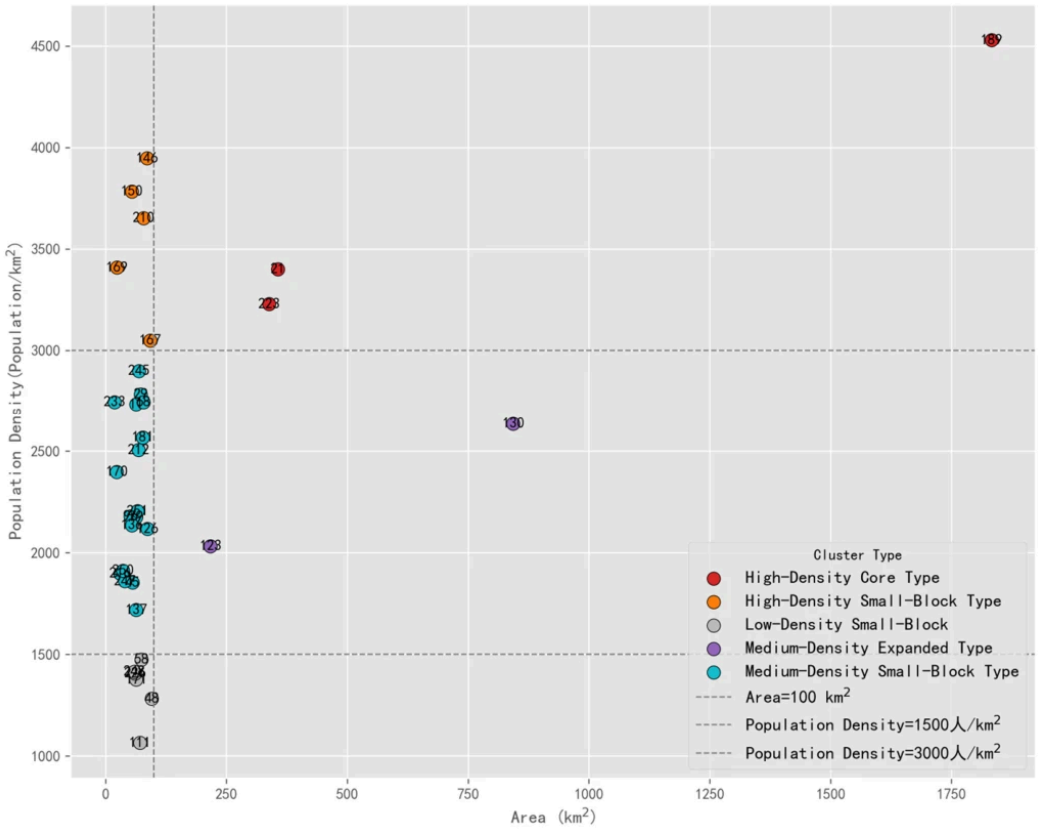


Figure 3. Quadrant diagram of vitality-cluster typology by area and population density.

According to the spatial distribution of vitality clusters in Figure 4, High-density large-area clusters mainly include #189, #21, and #223. Among them, #189 crosses Nanjing and Ma'anshan and covers the main urban area of Nanjing and northern Ma'anshan, demonstrating cross-administrative high-vitality integration. Cluster #21 is concentrated in the central urban area of Huai'an, indicating that a medium-sized city can also form a highly agglomerated local main center. Cluster #223 is located in the central urban area and southern new-town area of Ma'anshan, extending in a north–south strip and representing a typical riverside industrial–living mixed belt.

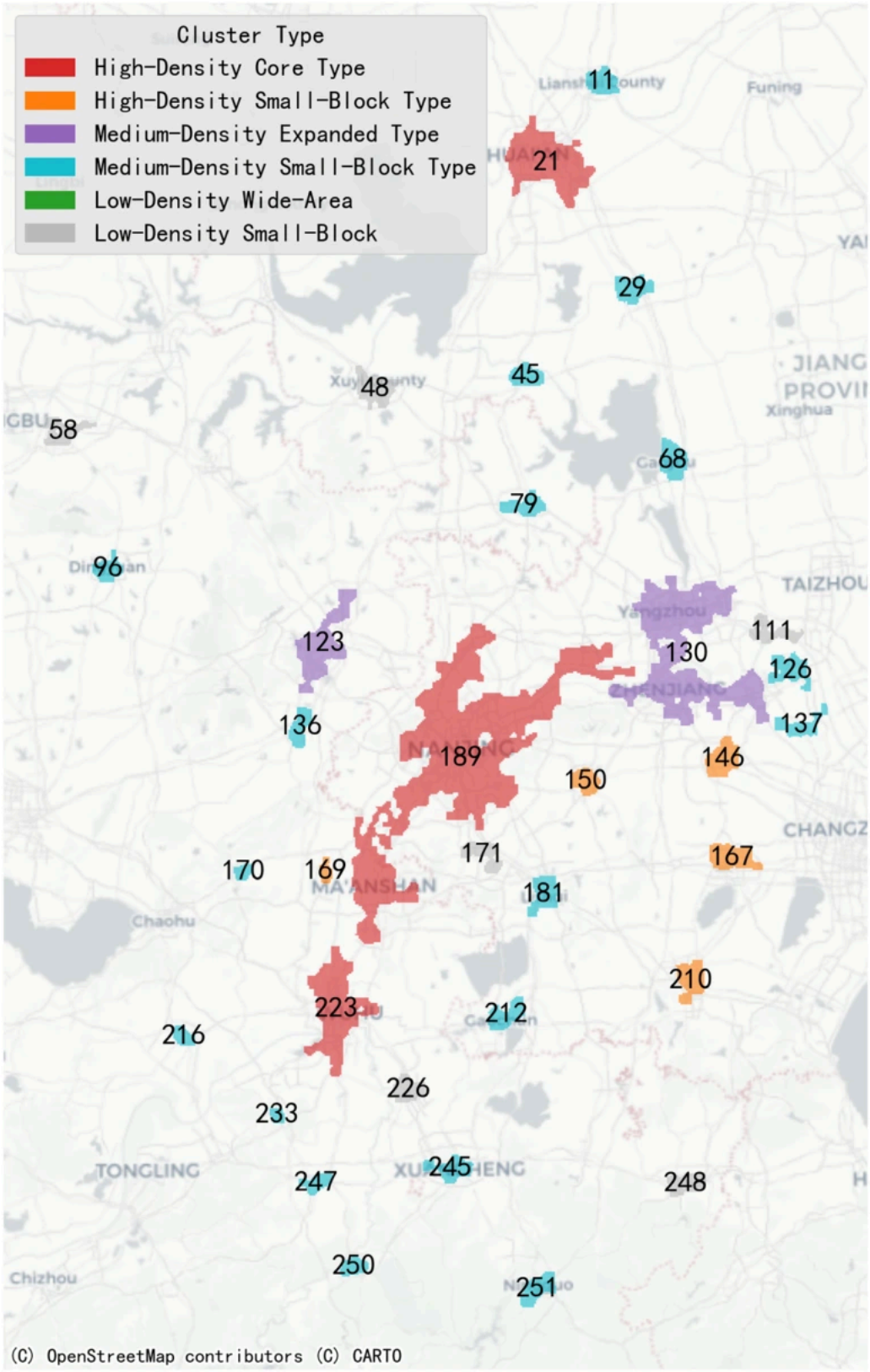


Figure 4. Spatial distribution of typed vitality clusters.

Medium-density large-area clusters are spatially extensive and in some cases span multiple urban centers. For example, Cluster #130 extends across Zhenjiang and Yangzhou, indicating a spatially continuous pattern across the two urban areas. Cluster #123 is located in the core area of Chuzhou and exhibits a clear north–south extension.

Medium-density small-area clusters are the most numerous and widely distributed, occurring extensively in subcenters or district-level administrative centers; they constitute important local vitality supports in the Nanjing Metropolitan Area.

4.2. Internal Vitality Structure and Mean Cluster Vitality Intensity

As shown in Figure 5, the 34 vitality clusters generally exhibit an internal structure of "high-vitality core–low-vitality edge." In other words, vitality clusters are not homogeneous high-value areas, but activity-based spatial units containing internal layers such as cores, transition zones, and edges. Different clusters vary substantially in scale, morphology, boundary clarity, and upper vitality limit. Some clusters are compact, with well-defined cores and clear attenuation, while others are loose, boundary-complex, and characterized by multi-core or axial expansion.

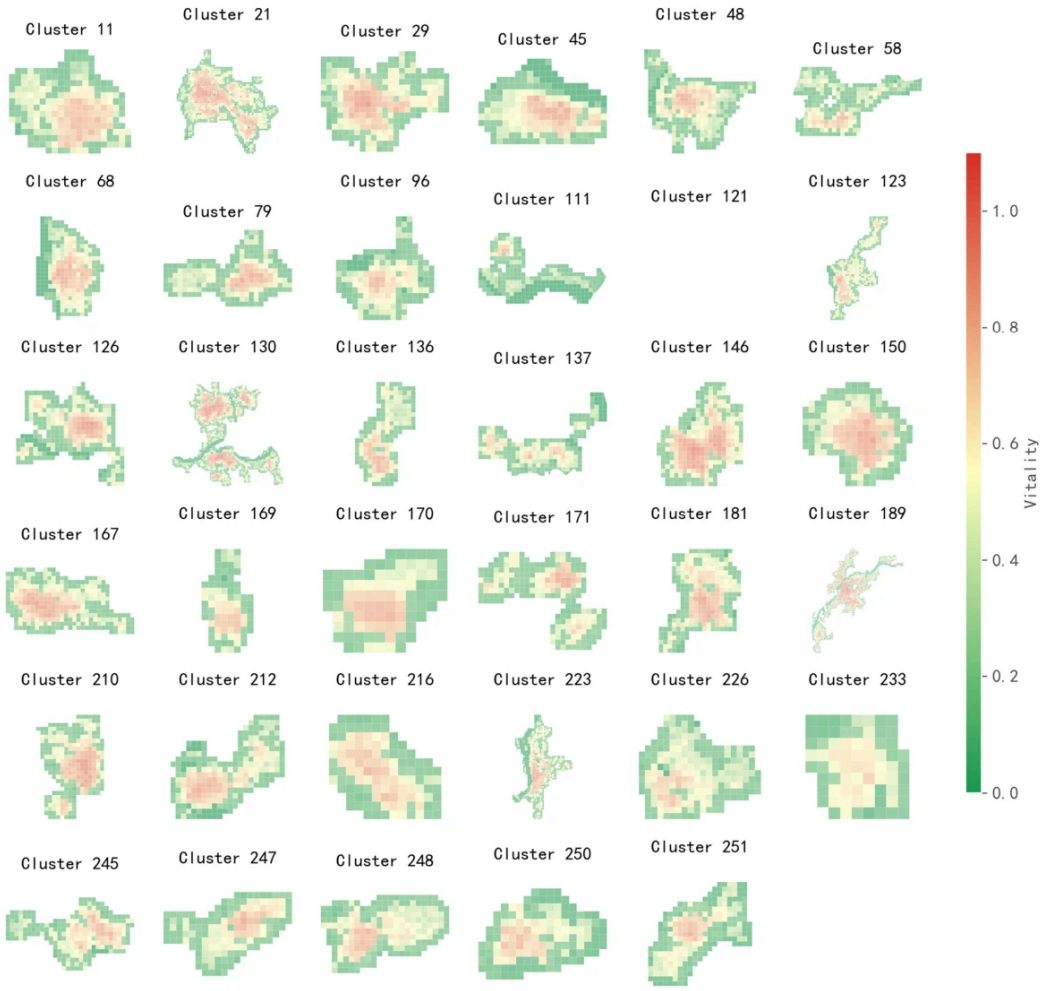


Figure 5. Internal vitality structure of the 34 vitality clusters.

Typical clusters further reveal these differences in internal organization. Cluster #189 is located in the Nanjing-Ma'anshan-Yangzhou metropolitan core belt, where vitality values form a north–south high-value belt and the core is concentrated in the main urban area of Nanjing. Cluster #130 links the main urban areas of Zhenjiang and Yangzhou and exhibits a dual-core outward attenuation structure. Cluster #123 forms a strip-like distribution in the main urban area of Chuzhou and contains local sub-cores beyond the main core. Clusters #146 and #150 show clearer center-edge structures, with high-value cores corresponding to government districts, high-tech zones, or industrial parks. Cluster #223 extends longitudinally along the Wuhu-Ma'anshan direction, indicat-

ing that transport axes and industrial–living mixed belts jointly shape its vitality organization.

As shown in Figure 6, all clusters have maximum vitality values above 0.7, and six exceed 0.95. Cluster #189 reaches the highest maximum value among all clusters, at 1.100; clusters such as #130, #146, and #21 also have high peak values. At the same time, clusters #189, #130, #21, #146, and #68 have high internal vitality standard deviations, indicating the coexistence of strong vitality cores and low-vitality edges. Clusters #111, #58, and #226 have lower standard deviations, indicating relatively stable vitality distributions but limited overall intensity. Detailed vitality information for all clusters is provided in Supplementary Table S14.

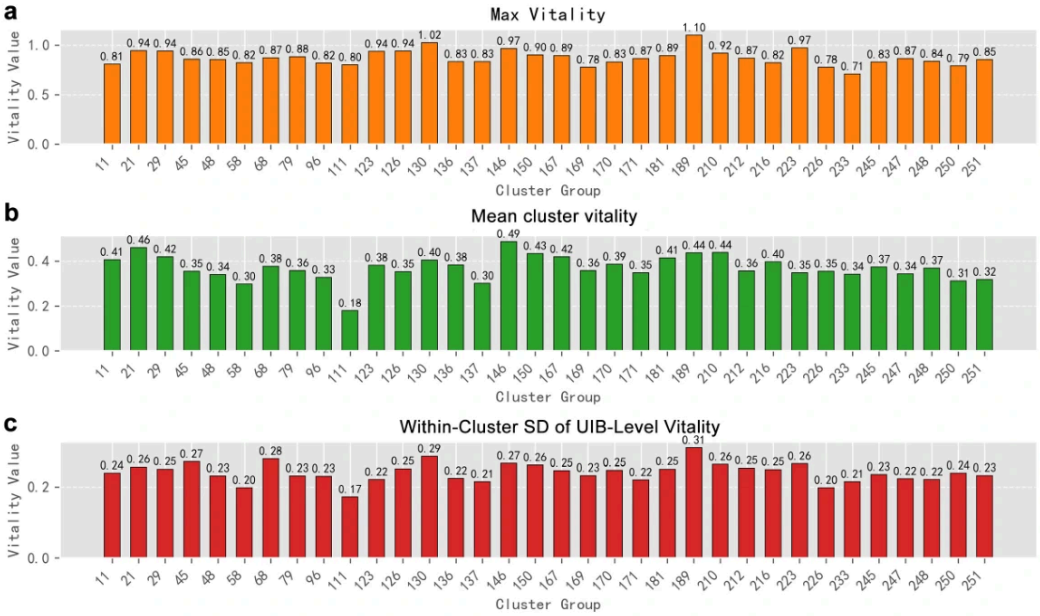


Figure 6. (**a**) Maximum UIB-level vitality within each cluster; (**b**) mean cluster vitality; (**c**) within-cluster standard deviation of UIB-level vitality.

4.3. Spatial Interpretability Assessment of Vitality Clusters as Activity-Based Spatial Units

Spatial interpretability was examined through four complementary perspectives: administrative-unit correspondence, cross-boundary extent, correspondence with built-up territories, and rank–size structure (see Table 4).

Table 4. Summary of supporting evidence for the spatial interpretability of vitality clusters.

Assessment Dimension	Assessment Method	Key Result	Relevance to the Research Logic
Spatial correspondence	Comparison with administrative-unit coverage	Core-district coverage reaches or exceeds 90%, while peripheral counties are mostly 2–15%	Shows spatial correspondence with high-coverage core areas
Boundary interpretability	Statistics of cross-administrative clusters	10 of 34 clusters cross county-level administrative units; #189 crosses 16 units	Describes the cross-boundary spatial extent of selected clusters
Coupling with built-up territories	Built-up-territory coverage and cross-territory statistics	17 built-up territories have coverage >0.7; only 4 of 34 clusters cross built-up territories	Shows that clusters are coupled with built-up space but not fully constrained by it

Assessment Dimension	Assessment Method	Key Result	Relevance to the Research Logic
Hierarchical structure	Descriptive rank–size comparison	Cluster area exponent ≈1.04; population exponent ≈1.26	Provides a descriptive comparison of scale hierarchy

First, vitality clusters show strong correspondence with high-intensity built-up areas and core functional areas. The results for county-level administrative-unit coverage show that central districts of Nanjing, such as Qinhuai, Gulou, Jianye, and Yuhuatai, have coverage rates that reach or approach 90%, whereas most peripheral counties have coverage rates of only 2–15%. This indicates that vitality clusters can capture actual high-vitality areas more precisely rather than simply replicating administrative boundaries.

Second, several of the final identified clusters extend across administrative boundaries. As shown in Figure 7a, 10 of the 34 clusters cross two or more county-level administrative units, accounting for 29.4%; among them, #189 crosses 16 administrative units, #130 crosses 9, and #223 crosses 5. These results describe the cross-administrative spatial extent of the final operational clusters rather than independently demonstrating the continuity of the underlying unprocessed vitality surface. This indicates that some high-vitality spaces do not conform to administrative boundaries, but are continuously organized along transport linkages, functional corridors, and contiguous urbanized areas. Detailed statistics are provided in Supplementary Tables S2 and S3.

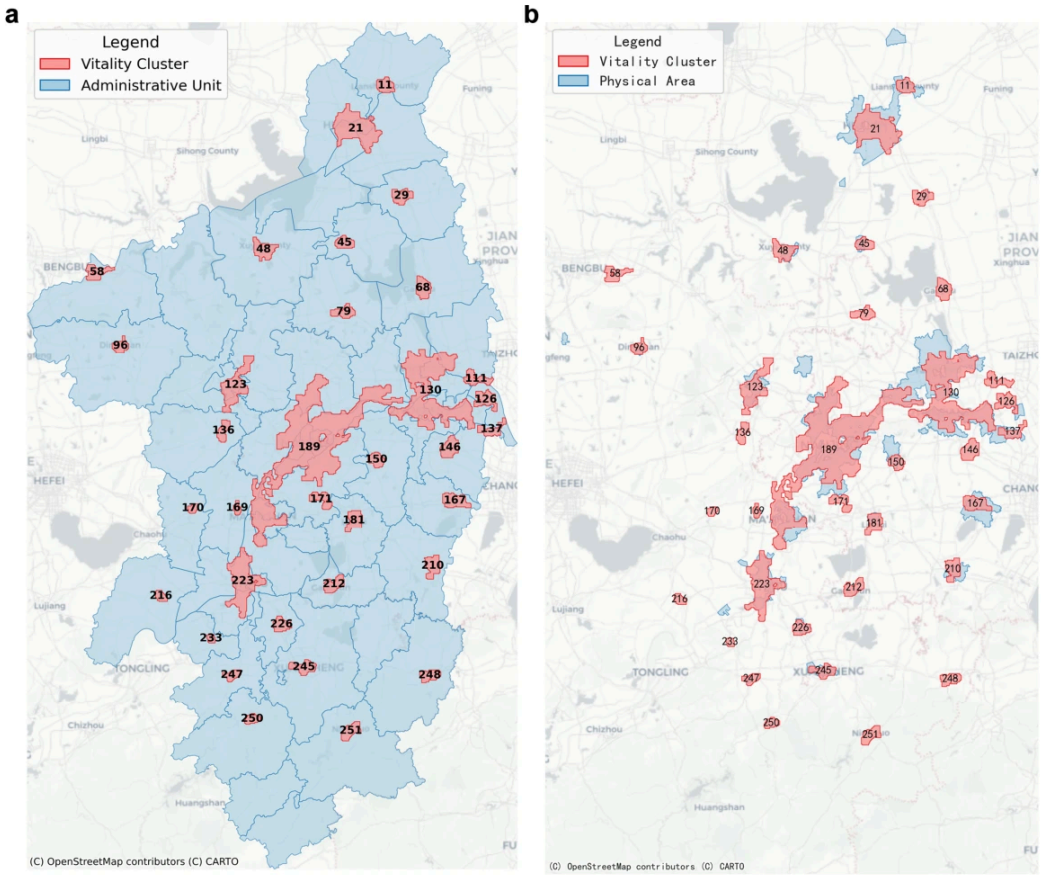


Figure 7. (**a**) Overlap between vitality clusters and administrative units; (**b**) overlap between vitality clusters and built-up territories.

Third, vitality clusters show substantial spatial correspondence with built-up territories. As shown in Figure 7b, 17 built-up territories have cluster coverage rates above 0.7, accounting for 58.6%; at the same time, only 4 vitality clusters cross built-up territo-

ries, accounting for 11.8%. This indicates that vitality clusters maintain a high correspondence with continuous built-up space while also identifying differences in actual activity intensity within built-up territories. Detailed statistics are provided in Supplementary Table S4 and Table S5.

Finally, the three spatial-unit systems exhibit different rank–size patterns in terms of area and population. For this descriptive comparison, units were ranked in descending order by area or population, and the corresponding rank–size relationships were fitted by linear regression in log–log space. The fitted slope was used as the rank–size exponent, with values closer to the canonical Zipf value of 1 indicating a distribution more similar to the classical rank–size relationship. As shown in Figure 8, the area and population exponents of the vitality clusters are approximately 1.04 and 1.26, respectively, compared with 0.88 and 0.53 for administrative units and 1.97 and 2.16 for built-up territories. Given the limited number of vitality clusters (N = 34) and the unequal sample sizes across the three spatial-unit systems, these fitted exponents are interpreted only as descriptive indicators of scale hierarchy rather than as formal evidence that the datasets follow a true Zipf or power-law distribution.

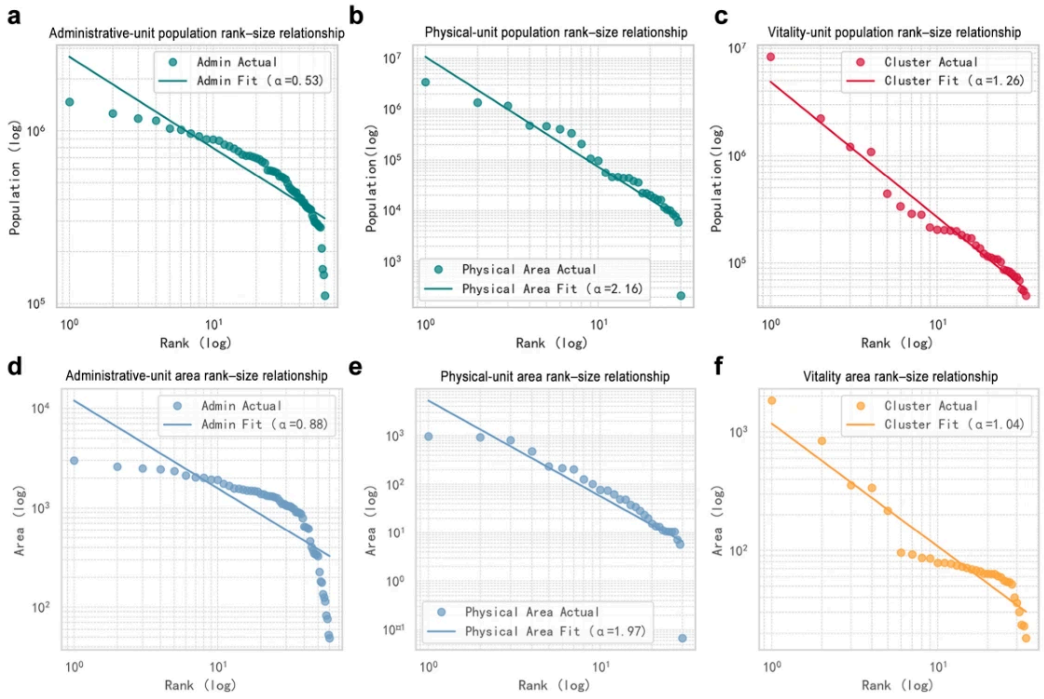


Figure 8. Rank–size relationships of population and area across different spatial-unit systems. (a) Administrative-unit population rank–size relationship; (b) physical-unit population rank–size relationship; (c) vitality-cluster population rank–size relationship; (d) administrative-unit area rank–size relationship; (e) physical-unit area rank–size relationship; (f) vitality-cluster area rank–size relationship. Points denote observed values, solid lines indicate the fitted power-law relationships on log–log scales, and \(\alpha\)denotes the fitted scaling exponents

Road structure reflects the basic conditions for internal spatial linkage and activity flow within vitality clusters, and Table 5 presents the indicator results for representative clusters. Cluster #189 has the largest road system, with a total road length of 8737.840 km, 49,221 road segments, and a road density of 4.766 km/km^2, showing that this metropolitan core cluster combines high vitality with an extensive road network. Cluster #130 has a total road length of 3438.960 km, indicating a broad road-network extent in the Zhenjiang–Yangzhou composite area. Although #170 is small in area, its road density

reaches 12.008 km/km^2, showing that high local road density can also occur in small-scale vitality clusters. Full results are provided in Supplementary Table S6.

Table 5. Basic road-structure indicators of representative vitality clusters.

Cluster ID	Cluster Area (km^2)	Total Road Length (km)	Average Segment Length (km)	Road Density (km/km^2)	Dominant-Direction Ratio	Weighted Directional Standard Deviation
21	356.500	1298.730	0.334	3.643	0.119	57.04
45	55.500	216.480	0.279	3.901	0.236	59.90
111	70.897	189.073	0.256	2.667	0.109	55.50
123	217.000	701.246	0.381	3.232	0.144	55.40
146	85.500	503.099	0.194	5.884	0.145	56.76

The road-structure typology further indicates that vitality clusters are commonly characterized by a "medium-density–weak-axis-mixed" structure. Clusters #126, #170, and #189 belong to the "high-density–no-axis-mixed" type, suggesting that although core areas have high road density, their directional organization is relatively complex. Peripheral clusters such as #111, #212, and #251 exhibit a "low-density–no-axis-mixed" structure, indicating that their road organization and vitality support still need improvement. Overall, higher road density tends to co-occur with higher vitality levels, while directional organization and network regularity further differentiate the spatial profiles of the clusters.

4.4. Geometric-Form Characteristics

Geometric form reveals the compactness, boundary regularity, and expansion mode of vitality clusters, and Table 6 presents the indicator results for representative clusters. The compactness of the 34 clusters ranges from 0.048 to 0.708, showing significant differences. Among them, #233 and #216 have high compactness values of 0.708 and 0.608, respectively, indicating regular forms and high spatial-organization efficiency. Cluster #189 has a compactness value of only 0.048, while its fractal dimension reaches 1.257 and its boundary complexity reaches 4.559; both are the highest values in the sample. This indicates that although #189 is a high-vitality core cluster, its spatial form is characterized by broad expansion, multi-core aggregation, and complex boundaries. The result shows that high vitality does not necessarily correspond to high compactness. For super-large core clusters, complex boundaries and multi-centered organization may themselves be spatial outcomes of continuous regional vitality expansion. Full results are provided in Supplementary Table S7.

Table 6. Basic geometric-form indicators of representative vitality clusters.

Cluster ID	Compactness Index	Fractal Dimension	Boundary Complexity
21	0.273	1.194	1.912
45	0.569	1.174	1.325
111	0.214	1.225	2.163
123	0.196	1.217	2.260
146	0.555	1.171	1.342

4.4.1. Distribution and Agglomeration Characteristics

Distribution and agglomeration characteristics are used to explain the spatial cohesion, core displacement, and axial organization of vitality clusters, and Table 7 presents the indicator results for representative clusters. The results show that #21 and #130 have relatively high centrality values of 11,024.742 m and 17,372.510 m, respectively.

Table 7. Basic distribution and agglomeration indicators of representative vitality clusters.

Cluster ID	Centrality	Hollowness	Dominant-Direction Angle	Distribution Type
21	11,024.742	0.000	118.301	Mixed
45	4308.810	0.000	90.000	Concentrated
111	5553.752	0.011	111.648	Mixed
123	9683.657	0.000	40.764	Dispersed
146	5271.520	0.000	0.000	Concentrated

In terms of spatial type, concentrated clusters such as #11, #45, and #146 show higher spatial aggregation and more regular boundaries. Mixed clusters, including #68, #79, and #210, are numerous and represent typical urban development zones. Dispersed clusters such as #123, #130, and #223 are spatially extensive and morphologically loose, reflecting trends of polycentric development and axial expansion. Thus, vitality clusters may appear as compact cores or as composite structures formed along transport corridors or urban expansion directions. Full results are provided in Supplementary Table S8.

4.4.2. Accessibility and Connectivity Characteristics

Accessibility and connectivity characterize the topological continuity and organization of the road network within vitality clusters. Table 8 reports the corresponding indicators for the representative cases. Node coverage equals 1 for all clusters, indicating that the retained road graphs are represented by a single dominant connected structure. Random-walk average step length varies substantially among clusters and is generally larger in spatially extensive road networks; it is therefore interpreted together with cluster scale and other connectivity indicators rather than as an independent measure of accessibility.

Table 8. Basic accessibility and connectivity indicators of representative vitality clusters.

Cluster ID	Random-Walk Average Step Length (Steps)	Node Coverage (Proportion)	Number of Connected Subgraphs (Count)	Average Degree (Dimensionless)	Graph Density (Dimensionless)
21	2127	1	1	2.15013	0.00010
45	350	1	1	2.18820	0.00062
111	364	1	1	2.13158	0.00058
123	875	1	1	2.16648	0.00025
146	1144	1	1	2.17341	0.00019

The connectivity results show that medium- and small-city clusters such as #233, #216, #169, and #96 have relatively high graph densities, characterizing comparatively compact network configurations. By contrast, large-scale clusters such as #189 and #130 have lower graph densities but larger network extents. Therefore, connectivity indicators should not be interpreted simply by graph density; rather, they should be considered together with cluster scale, total road-network size, and core-organization mode. Full re-

sults are provided in Supplementary Table S9.

4.4.3. Functional Diversity, Balance, and Core-Area Functional Agglomeration

Functional diversity and balance explain the degree of functional supply complexity and structural rationality within vitality clusters, and Table 9 presents the indicator results for representative clusters. The functional mix of the 34 clusters ranges from 1.69 to 2.11, and functional balance ranges from 0.64 to 0.80. High values are mainly concentrated in the core areas of the Nanjing Metropolitan Area and in clusters belonging to central cities. Among them, #189 has a functional mix value of 2.112 and a functional balance value of 0.800, making it the cluster with the most complex and balanced functional structure. Clusters #130, #212, and #223 also have relatively high functional balance. By contrast, #248, #233, and #250 have lower functional mix and balance values, indicating relatively simple functional structures. Overall, functional diversity is an internal support for the formation of urban vitality; areas with more diverse and more balanced functions tend to have higher vitality values. Functional completion and mixing in urban-edge clusters are therefore important entry points for enhancing regional vitality. Full results are provided in Supplementary Table S10.

Table 9. Basic functional indicators of representative vitality clusters.

Cluster ID	Functional Mix	Functional Balance
21	1.95612	0.74122
45	1.92867	0.73082
111	1.78051	0.67468
123	1.90400	0.72147
146	1.91370	0.72514

Core-area functional agglomeration further shows that different clusters have different modes of functional organization. Medium- and small-scale clusters such as #233, #170, and #216 concentrate multiple functions in their core areas, reflecting the characteristics of compact central urban areas. In contrast, although #189, #130, and #223 have high overall vitality and functional complexity, their functions are more dispersed within the clusters, indicating that their vitality depends more on large-scale comprehensive support than on single-core agglomeration. Clusters with strong functional agglomeration are more likely to exhibit clear core-vitality guiding structures, which are conducive to resource concentration and efficiency improvement. Functionally dispersed clusters need network linkage, node organization, and continuous-interface construction to reduce vitality loss caused by functional dispersion. Related full results are provided in Supplementary Tables S11 and S12.

Taken together, the five dimensions reveal substantial variation in the spatial organization of vitality clusters. Table 10 synthesizes the principal morphological patterns and their interpretive relevance.

Table 10. Summary of key results on multi-dimensional spatial morphology.

Dimension	High-Value/ Typical Clusters	Key Result	Interpretive Meaning
Road structure	#189, #130, #170	#189 has a total road length of 8737.840 km; #170 has a road density of 12.008 km/km^2	Broad core clusters are characterized by extensive road networks, whereas small-scale clusters can

Dimension	High-Value/ Typical Clusters	Key Result	Interpretive Meaning
			exhibit high local road density.
Geometric form	#233, #216, #189	#233 has compactness of 0.708; #189 has compactness of 0.048 and boundary complexity of 4.559	High vitality does not necessarily correspond to high compactness
Distribution and agglomeration	#21, #130, #123	#21/#130 have high centrality; #123/#130/#223 are dispersed or axially expanded	Clusters may be concentrated, mixed, or dispersed in organization
Accessibility and connectivity	#189, #130, #233	#189 has a random-walk average step length of 18,551; #233 has a relatively high graph density	Large clusters tend to exhibit broader road networks, whereas medium and small clusters show more compact network configurations.
Functional structure	#189, #130, #233	#189 has H = 2.11206 and E = 0.80031; #233 shows strong core functional agglomeration	Functional diversity and core agglomeration co-occur with differentiated vitality profiles across clusters.

4.5. Type Differences and Representative Cluster Profiles

4.5.1. Statistical Differences Among Cluster Types

To examine whether the operationally defined cluster groups exhibit systematic differences in their functional, morphological, transport, economic, and ecological characteristics, inter-group comparisons were conducted across 60 non-redundant variables. After Benjamini–Hochberg FDR correction, 30 variables (50.0%) remained significant. These comprised 15 functional, 7 transport, 5 morphological, and 3 economic variables, whereas no ecological variable remained significant after correction (Table 11). Functional variables therefore constitute the largest group of differentiating characteristics, followed by transport and morphological variables. An additional robustness analysis in which all 60 variables were tested using Kruskal–Wallis retained 25 FDR-significant variables, all of which were included in the primary set of 30. These results provide exploratory evidence of multidimensional differentiation among the operationally defined groups. Given the small and uneven group sizes, the statistical results are interpreted as within-sample inter-group comparisons rather than as confirmatory validation of the grouping. Full test statistics, raw and FDR-adjusted *p*-values, effect sizes, robustness results, and post hoc comparisons are provided in Supplementary Tables S13, S18 and S19.

Table 11. Summary of factors remaining significant after BH-FDR correction.

Factor Category	Number Significant After BH-FDR	Representative FDR-Significant Factors	Role in Type Interpretation
Functional	15	Cultural entertainment, residential services, economic services, transport services, innovation, catering entertainment, POI density, functional mix	Distinguishes functionally complex/high-vitality groups from functionally insufficient groups

Factor Category	Number Significant After BH-FDR	Representative FDR-Significant Factors	Role in Type Interpretation
Morphological	5	Compactness, building-age diversity, centrality, boundary complexity, fractal dimension	Describes differences in spatial organization and boundary form
Transport	7	Parking density, intersection density, total road length, random-walk step length, graph density, road-segment count, public-transit stop density	Describes transport/network support and activity-flow conditions
Economic	3	Nighttime light intensity, GDP, average housing price	Reflects economic activity and market attractiveness
Ecological	0	—	No ecological factor remained significant after BH-FDR correction

The spatial-dependence assessment showed that six of the 60 variables retained significant global spatial autocorrelation after FDR correction. None overlapped with the 30 variables that remained significant in the primary inter-group analysis, indicating that the principal group differences were not concentrated in variables showing detectable global spatial dependence under the specified four-nearest-neighbour weights (Supplementary Table S17).

To visualize the multidimensional profiles of the cluster groups, 12 representative factors were selected from the revised statistical results to construct standardized mean radar charts. As shown in Figure 9, High-density large-area clusters perform strongly in intersection density, parking density, innovation-service level, GDP, functional balance, centrality, nighttime light intensity, and building-age diversity, indicating that their vitality is jointly shaped by transport support, functional complexity, economic intensity, and spatial diversity. High-density small-area clusters have advantages in POI density, cultural and entertainment service level, and compactness index, reflecting a local vitality mechanism of "small scale–high density–strong hot spots." Medium-density large-area clusters show relatively high building-age diversity and nighttime light intensity, indicating heterogeneous built-environment and activity characteristics across their larger spatial extent. Medium-density small-area clusters have local advantages in compactness. Low-density small-area clusters mainly show prominent ecological attributes but insufficient economic, functional, and transport support.

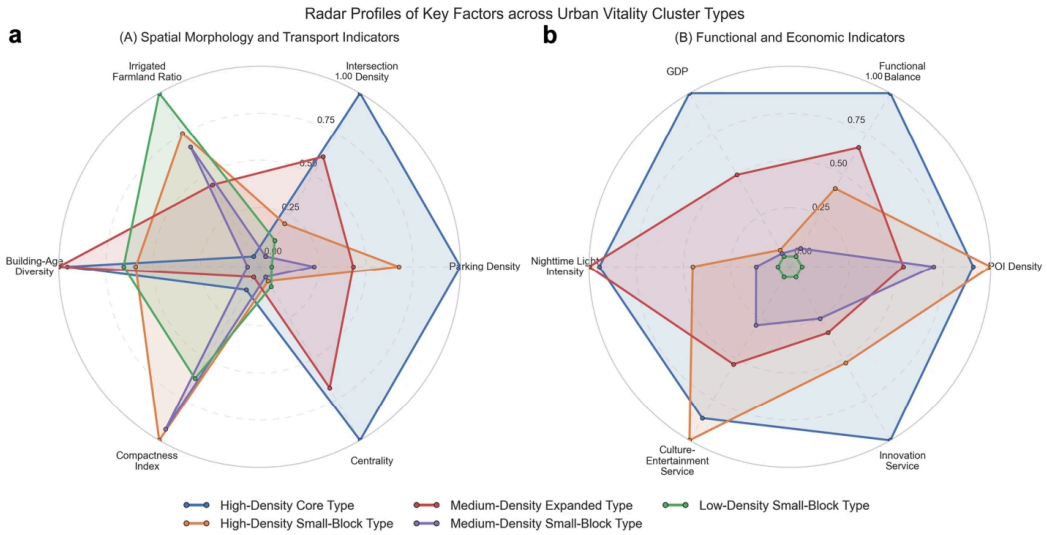


Figure 9. Standardized mean radar profiles of representative factors across the operational vitality-cluster groups. (a) Spatial-morphology and transport indicators; (b) functional and economic indicators. Colored profiles represent the five operational area–density groups

The boxplots and violin plots further reveal the degree of dispersion within different cluster types; see Figure 10 and Figure 11.Overall, transport and economic factors clearly distinguish the advantages of High-density large-area clusters. Functional factors show more complex type differences, indicating that clusters at the same density level may still have different modes of functional organization. Morphological and ecological factors reveal internal heterogeneity and edge attributes. Given the small and uneven group sizes, the violin plots are used descriptively to visualize the observed within-group dispersion; multimodal or long-tailed shapes are not interpreted as evidence of latent subgroups or different developmental stages.

On the basis of these results, this study summarizes the representative clusters of different cluster types. High-density large-area clusters are the vitality cores of the metropolitan area, with high transport accessibility, functional complexity, economic activity, and spatial diversity, but they also face problems of boundary complexity, internal heterogeneity, and pressure on public space. High-density small-area clusters are local vitality hot spots, with dense POIs, prominent cultural and entertainment functions, and compact blocks, but their stability needs to be enhanced through multi-axis connections and frontage continuity. Medium-density large-area clusters constitute secondary centers and peripheral vitality belts, with regional linkages and transitional spatial attributes, but discontinuous interfaces and inefficient edges should be repaired. Medium-density small-area clusters are mostly local living spaces, with relatively compact forms but limited functional support. Low-density small-area clusters can serve as ecological buffers and potential cultivation areas.

4.5.2. Representative Cluster Case Profiles

On the basis of the preceding inter-group and morphological analyses, the five purposively selected representative clusters (#21, #45, #111, #123, and #146) are examined to illustrate how group-level differences are expressed within specific spatial units. Unlike the preceding statistical comparison, the case profiles focus on road networks, building texture, functional agglomeration, boundary form, and activity-support structures within individual clusters.

Figure 12 shows that representative clusters are not homogeneous patches but have distinct spatial-organization profiles. High-density clusters tend to form composite ac-

tivity cores supported by continuous built-up environments, complete road networks, and dense functional points; medium-density clusters more often display axial extension, grouped articulation, or local corridor-like structures; and low-density clusters are more nodal and fragmented. Specifically, #21 and #146 both show strong road–building–function coupling, but #21 represents a multi-node composite core, whereas #146 is a small-scale, highly agglomerated unit. Clusters #123 and #45 respectively reflect broad expansion and linear-corridor organization, while #111 illustrates node dispersion and weak interface continuity. These results suggest that cluster types differ not only in area and population density, but also in spatial continuity, functional-node organization, road-support mode, and boundary form.



Figure 12. Spatial configuration of the five representative vitality clusters. (a) Cluster #21; (b) Cluster #123; (c) Cluster #45; (d) Cluster #111; (e) Cluster #146. Buildings, POIs, roads, and cluster boundaries are shown to illustrate the spatial organization of each representative case

Figure 13 further clarifies the diagnostic value of typical cases by comparing each case with the mean profile of its own type.High-density cases generally show advantages in functional density, service complexity, and nighttime activity support, but may still have weaknesses in transport capacity, functional structure, or spatial organization. Medium-density cases show more differentiated patterns, either relying on compact or linear morphology to support local vitality, or retaining transport and nighttime-activity

advantages while lacking functional complexity, higher-order services, and node continuity. Low-density cases reveal that their key limitation is not merely low development intensity, but insufficient network linkage, functional mix, and continuous active interfaces. Thus, Figure 13 demonstrates that intra-type differences remain substantial, and that vitality clusters require case-specific diagnosis beyond type identification.

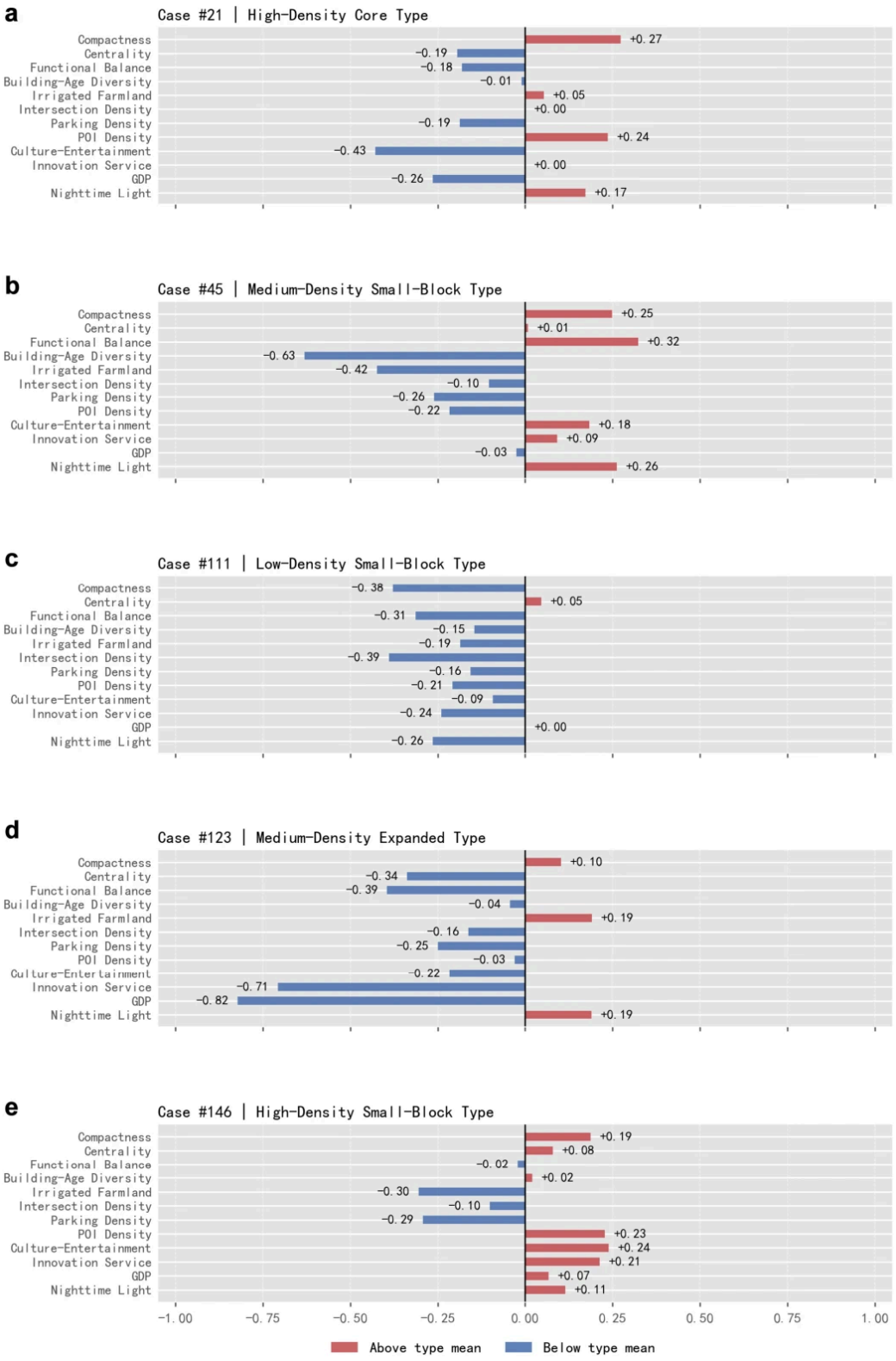


Figure 13. Relative deviations of representative cases from their corresponding operational-group means. (a) Cluster #21, High-Density Large-Area; (b) Cluster #45, Medium-Density Small-Area; (c)

Cluster #111, Low-Density Small-Area; (d) Cluster #123, Medium-Density Large-Area; (e) Cluster #146, High-Density Small-Area. Positive values indicate values above the corresponding group mean, whereas negative values indicate values below the group mean

Taken together, Figures 12 and 13 provide two complementary forms of evidence. The spatial morphological profiles reveal how typical clusters are organized in real space, whereas deviations from the corresponding type mean identify the dimensions in which each case is stronger or weaker than the average level of its type. By combining these two forms of evidence, vitality clusters are no longer merely statistical type labels, but can be further transformed into diagnostic units for urban regeneration. On this basis, Table 12 summarizes the spatial characteristics, major problems, and planning directions of the typical clusters.

Table 12. Spatial profiles, problem diagnosis, and potential planning implications of representative clusters.

Type	Representative Clusters	Main Characteristics	Main Problems	Potential Planning Implication
High-density large-area	#21/#189	High functionality, strong transport support, strong core	Overload and boundary complexity	Public-space pressure relief and branch-road supplementation
High-density small-area	#146	Small scale, high density, strong agglomeration	Limited spatial carrying capacity	Pocket infill and frontage continuity
Medium-density large-area	#130/#123	Broad expansion and multi-core linkage	Loose boundaries and dispersed functions	Node cultivation and main-axis repair
Medium-density small-area	#45	Potential for linear corridors	Insufficient vitality hierarchy	Dual-line organization and block stitching
Low-density small-area	#111/#248	Low-density, ecological, or peripheral attributes	Weak functional and transport support	Functional introduction and slow-mobility network supplementation

4.6. Micro-Scale Case Examination: Block Morphology, Continuous Interfaces, and Walkability

To further examine how the cluster-level differences identified above are expressed at the urban-design scale, this section conducts a micro-scale case examination of the five representative clusters. The analysis uses block grain, street-frontage continuity, continuous commercial frontage, local mixed-use intensity, and walkability to interpret how different cluster profiles are manifested in finer-scale spatial conditions.

First, block-morphology indicators show that different cluster types have clear differences in their micro-scale spatial skeletons. The results show obvious differences in street-frontage continuity and street-edge density across cluster types, as shown in Figure 14 a,b. According to Table 13, #146 presents a typical "small-block–high-interface–compact organization" structure: the median block area is 3.6 ha, the proportion of small blocks is 31.0%, the median street-frontage continuity is 0.104, and the proportion of high-continuity blocks is 31.9%. This indicates that High-density small-area clusters can form a strong street-interface basis within a limited spatial scale. Although #45 does not have a prominent proportion of small blocks, its proportion of high-continuity blocks reaches 26.9%, forming a linear vitality corridor that "wins through interface continuity." By contrast, #111 and #123 show weaker continuous support in block scale, building

spacing, and frontage continuity, reflecting that low-density or expanded clusters are more prone to dispersed functional nodes, broken interfaces, and insufficient pedestrian connections. Therefore, block morphology provides an important spatial context within which continuous activity can occur.

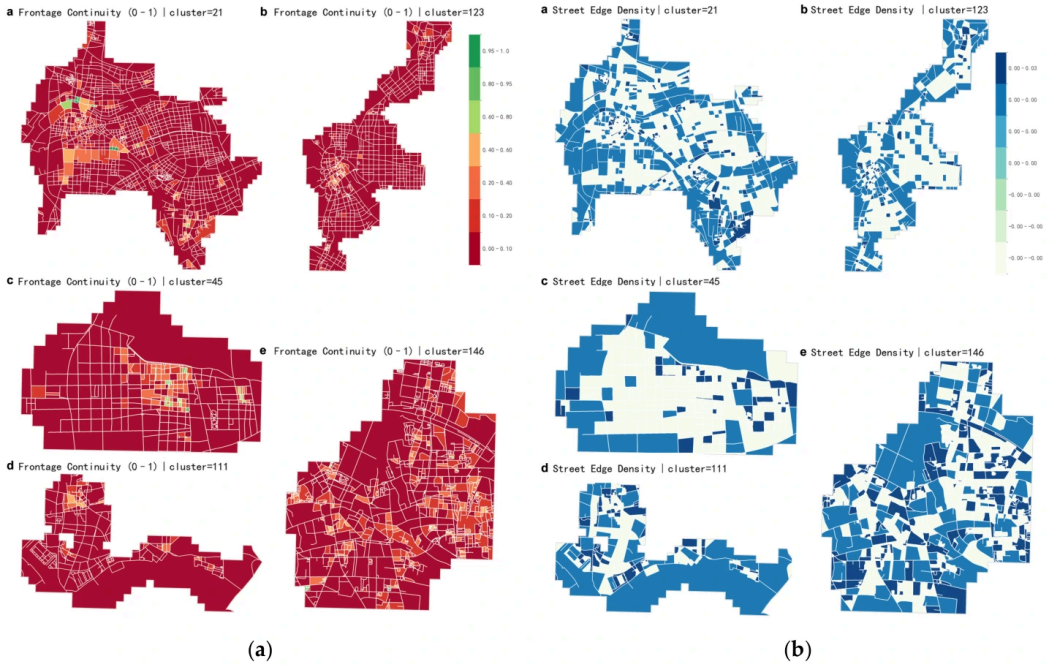


Figure 14. (**a**) Street-frontage continuity of representative clusters. (**b**) Street-edge density of representative clusters.

Table 13. Key block-morphology indicators of the five clusters.

Cluster ID	146	45	111	21	123
Number of blocks	872	279	222	1217	646
Median frontage continuity	0.104	0.044	0.035	0.012	0.004
Share of high-continuity blocks (≥citywide Q75)	31.90%	26.90%	17.10%	15.00%	13.20%
Median block area (ha)	3.6	10.4	9.3	18.7	23
Share of small blocks (≤citywide Q25)	31.00%	6.80%	15.80%	6.00%	6.80%
Approximate median building spacing (m)	47	55	66	62	72
Share of small spacing (≤citywide Q25)	28.40%	24.40%	19.40%	15.40%	14.40%
Share of high street-edge density (≥citywide Q75)	28.70%	17.90%	37.40%	25.80%	26.30%

Second, the functional-distribution results further show that the observed micro-scale vitality patterns co-occur with differences in functional mix, continuous commercial frontage, and active street-fronting interfaces. The local mixed-use levels of the five cases are all relatively high, indicating that representative clusters generally have a certain basis of functional complexity. However, the cases differ significantly in continuous commercial frontage length, the proportion of street-fronting and active buildings, and hot-spot organization, as shown in Figure 15a,b. According to Table 14, #21 has a continuous commercial frontage length of 8.88 km, a high-mix proportion of 95.10%, and a total hot-spot area of 887.61 ha. It therefore has long continuous commercial frontages and large functional hot spots, reflecting a composite support structure of "high mix–multiple cores–long interfaces." Clusters #45 and #146 respectively show linear interface agglomeration and pocket-like interface stitching, indicating that medium- and small-scale clusters can also form strong street vitality through locally continuous interfaces. Although #111 contains local functional points, its continuous commercial frontage is only 1.12 km, indicating that its active interfaces are insufficient and that it is difficult to form continuous street activity belts. Thus, functional mix can be translated into micro-scale vitality only when it is combined with accessible street interfaces and continuous walking paths.

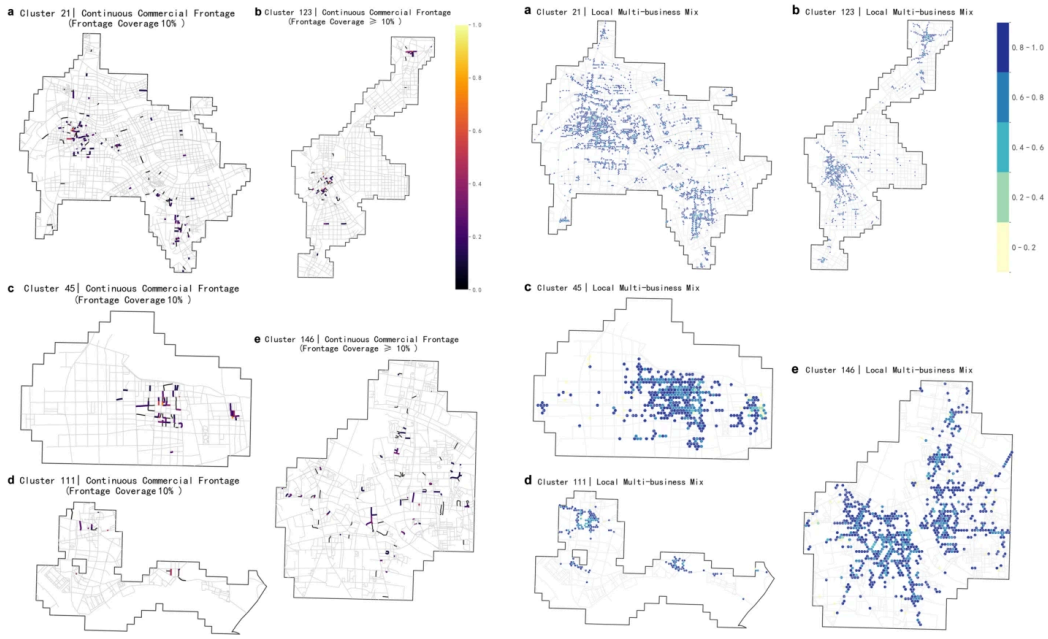


Figure 15. (**a**) Continuous commercial frontage of representative clusters. (**b**) Local mixed-use intensity of representative clusters.

Table 14. Key functional-distribution indicators of the five clusters.

Cluster ID	21	45	111	123	146
Total number of buildings	104,238	9139	12,917	46,224	29,468
Number of street-fronting buildings	15,121	2643	2460	6712	8280
Number of active-POI buildings	4590	686	509	1719	1750
Number of street-	3742	592	457	1414	1434

Cluster ID	21	45	111	123	146
fronting and active buildings					
Street-fronting rate	14.50%	28.90%	19.00%	14.50%	28.10%
Active-POI rate	4.40%	7.50%	3.90%	3.70%	5.90%
Street-fronting and active rate	3.60%	6.50%	3.50%	3.10%	4.90%
Mean frontage coverage rate	0.70%	2.00%	0.60%	1.10%	0.80%
P90 frontage coverage rate	0.00%	3.60%	0.00%	0.00%	0.00%
Continuous commercial frontage length (km)	8.88	3.04	1.12	4.23	3.76
Mean entropy	0.84	0.8	0.81	0.83	0.82
Median entropy	0.88	0.86	0.86	0.87	0.87
High-mix proportion	95.10%	91.30%	88.90%	94.80%	93.50%
Number of hexagons	2426	427	171	820	842
Number of hot spots	28,299	3731	4867	16,573	6512
Total hot-spot area (ha)	887.61	117.02	152.66	519.82	204.25
Total POIs within the road buffer	31,971	6144	2345	11,550	10,734

The walkability analysis shows clear differences in pedestrian-environment conditions across the selected cases, alongside differences in block morphology and functional organization, as shown in Figure 16. According to Table 15, #21 has a high weighted mean WS and a high P90 value, indicating relatively high-quality pedestrian corridors within the cluster. Although #45 is small in overall scale, its good-road share is 54.7% and its excellent-road share is 32.6%, the highest among the five cases. This pattern indicates that continuous interfaces and linear functional agglomeration co-occur with relatively higher walkability in this medium- and small-scale case. Cluster #146 has small blocks and a high street-fronting rate, but its walkability remains moderate, indicating that compact form alone is not sufficient to ensure a high-quality walking environment; more continuous active interfaces and a more complete slow-mobility connection are still required. Cluster #123 has a certain basis of functional mix and commercial frontages, but its walkability shows a structural imbalance of a strong main corridor and weak side wings. Cluster #111 exhibits a typical low walkability level, or "cold street" state. Combined with the results on block morphology and functional distribution, these cases suggest that walking-experience conditions vary jointly with block scale, street-interface continuity, local functional mix, and pathway accessibility rather than with density or functional supply alone.

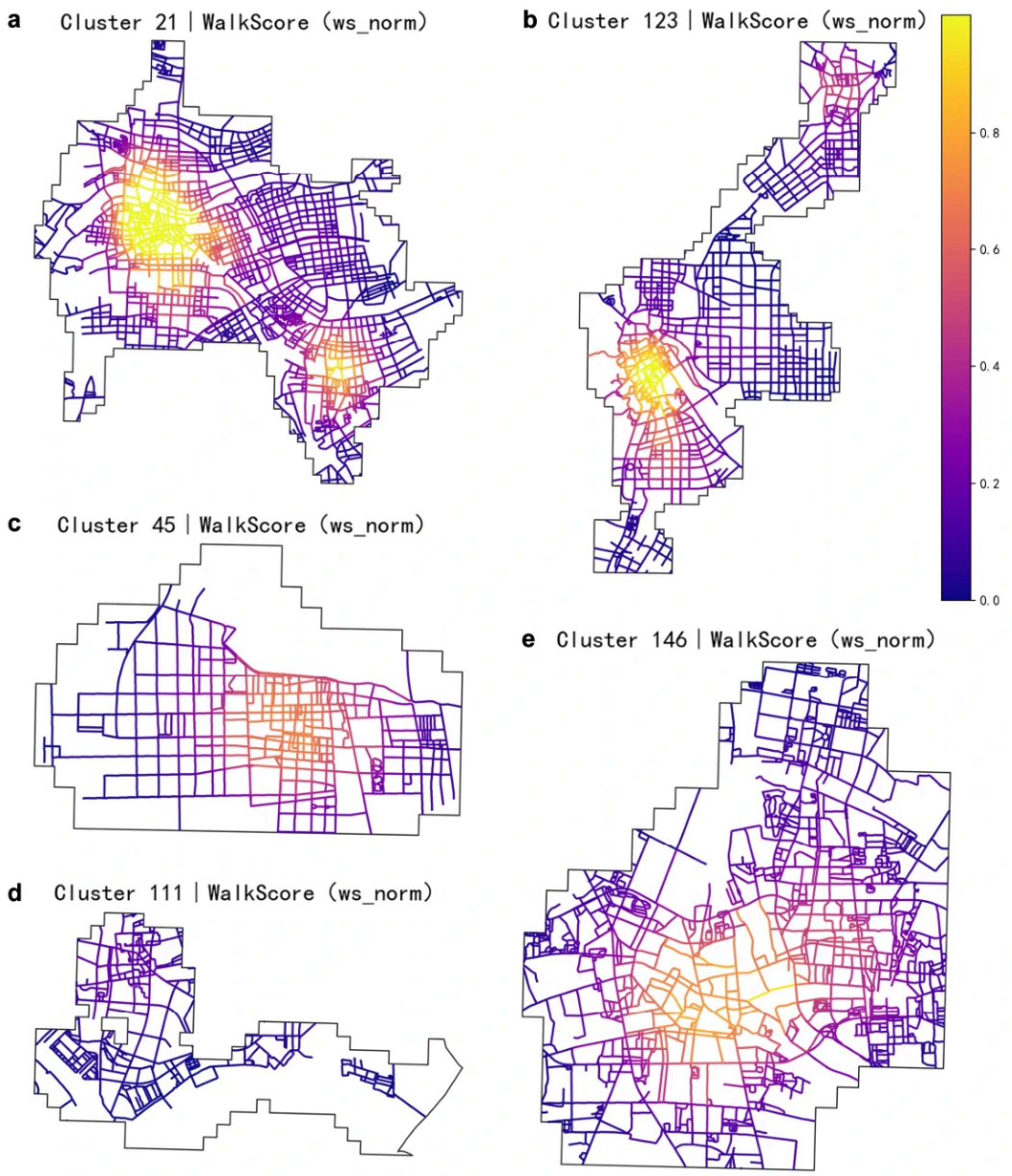


Figure 16. Spatial distribution of road-level walkability scores in the five representative vitality clusters. (a) Cluster #21; (b) Cluster #123; (c) Cluster #45; (d) Cluster #111; (e) Cluster #146. The color gradient represents the normalized walkability score, with higher values indicating greater pedestrian access to nearby facilities.

Table 15. Key walking-experience indicators of the five clusters.

Cluster ID	21	45	111	123	146
Total road length (km)	1429.11	247.41	208.55	792.73	581.68
Weighted mean WS	0.338	0.321	0.064	0.271	0.274
Percentile of mean WS	P76	P65	P3	P35	P38
Weighted WS P75	0.518	0.546	0.126	0.411	0.41
Percentile of WS P75	P65	P76	P3	P38	P35

Cluster ID	21	45	111	123	146
Weighted WS P90	0.846	0.655	0.165	0.717	0.584
Percentile of WS P90	P91	P53	P3	P65	P41
Share of ≥P80 WS segments	47.70%	54.70%	0.00%	39.60%	44.60%
Percentile of good-road share	P53	P65	P3	P32	P38
Share of ≥P90 WS segments	28.30%	32.60%	0.00%	20.60%	18.20%
Percentile of excellent-road share	P62	P82	P7	P44	P35

Note: WS denotes the road-level walkability score after 2nd–98th percentile robust normalization. ≥P80 and ≥P90 WS segments are defined using the metropolitan-wide 80th and 90th percentiles, respectively. Cluster statistics are weighted by road-segment length.

Overall, the micro-scale case examination illustrates three recurring relationships across the selected cases. First, block grain and street-frontage continuity constitute the morphological basis of micro-scale vitality, but they are not sufficient conditions. Second, local mixed-use intensity can be translated into continuous street activity only when it is organized through continuous commercial frontages and active ground-floor space. Third, walking-experience indicators provide an additional descriptive dimension for examining how morphological and functional conditions are expressed at the street scale. Therefore, the planning translation of vitality clusters should not remain at the level of increasing overall intensity or the quantity of functions. Instead, it should further identify micro-scale problems such as interface discontinuities, weak functional segments, slow-mobility gaps, and insufficient node connections.

From the perspective of type differences, the selected cases suggest several potential micro-scale priorities. High-density large-area clusters may benefit from maintaining multi-core continuity and improving public-space and slow-mobility conditions; High-density small-area clusters from connecting pocket-like active interfaces; Medium-density large-area clusters from strengthening main-axis continuity and lateral permeability; Medium-density small-area clusters from cultivating local living-oriented vitality corridors; and Low-density small-area clusters from improving basic services, slow-mobility networks, and local nodes rather than simply increasing development intensity. The key micro-scale indicators are summarized in Table 16. Thus, the micro-scale analysis provides potential diagnostic references for translating cluster-level morphological characteristics into urban-design and regeneration considerations.

Table 16. Key micro-scale indicators of the five clusters.

Cluster	Type	Block/Frontage Characteristics	Functional Characteristics	Walkability	Potential Planning Implication
#21	High-density large-area	Long continuous frontage	Continuous commercial frontage of 8.88 km; high-mix proportion of 95.10%	Mean = 0.338; P90 = 0.846	Maintain multi-core continuity and improve slow-mobility quality
#45	Medium-density	Strong linear	Active frontages	Good roads 54.7%;	Strengthen linear

Cluster	Type	Block/Frontage Characteristics	Functional Characteristics	Walkability	Potential Planning Implication
	small-area	frontage	agglomerate along the main axis	excellent roads 32.6%	corridors and node continuity
#146	High-density small-area	Small blocks, high street edge, pocket-like continuity	Street-fronting rate 28.10%; continuous commercial frontage 3.76 km	Moderate level; insufficient long segments	Pocket stitching and short-segment linkage
#111	Low-density small-area	Large, sparse, and discontinuous	Continuous commercial frontage 1.12 km	Mean = 0.064; good/excellent roads 0%	Node cultivation, functional introduction, and slow-mobility network supplementation
#123	Medium-density large-area	Strong main corridor and weak side wings	Continuous commercial frontage 4.23 km	Relatively strong but uneven main corridor	Main-axis break repair and lateral permeability improvement

5. Discussion

5.1. From Vitality-Intensity Measurement to Activity-Based Diagnostic Units

This study extends urban-vitality analysis from the measurement of activity intensity toward the construction and interpretation of activity-informed spatial units for regeneration diagnosis. Traditional urban vitality research usually focuses on the spatial distribution of vitality, hot-spot identification, and explanation of influencing factors [11] . However, if these results remain attached to administrative districts, regular grids, or block boundaries, their capacity for planning translation is limited [46]. The significance of vitality clusters lies in their integration of human activity, functional supply, road linkages, and spatial proximity into activity-based spatial units with continuous boundaries and internal structures [47].

Compared with studies that delineate functional areas or activity spaces from mobility, functional interactions, or individual behaviour [2,3,15,16,32–35], the vitality clusters examined here represent place-centred aggregations of observed urban vitality rather than individual or group activity spaces. The contribution therefore lies less in proposing another boundary-delineation technique than in treating vitality-derived clusters as spatial objects whose boundaries, internal morphology, and functional organization can be interpreted for regeneration diagnosis.

The results show substantial spatial correspondence between vitality clusters and built-up territories, while several clusters also extend across administrative boundaries. The rank–size comparison further indicates differences in scale hierarchy among vitality clusters, administrative units, and built-up territories [47]. Taken together, these analyses support the spatial interpretability of vitality clusters as activity-informed analytical units, without implying that the identified boundaries constitute a uniquely valid or scale-independent spatial delineation.

5.2. Multi-Scale Morphological Interpretability of Vitality Clusters

For the operationally defined cluster types, analysis of road structure, geometric form, distribution and agglomeration, accessibility and connectivity, functional mix, and micro-scale interfaces reveals clear and interpretable morphological differences. These

findings partly correspond to previous block- and street-scale studies linking compact urban form, functional diversity, and network accessibility with higher vitality [9,13,48,49]. However, the present results also qualify a simple assumption that higher vitality necessarily corresponds to greater compactness or morphological regularity. At the cluster scale, large metropolitan-core clusters can combine high vitality with low compactness, complex boundaries, and multi-centred spatial organization. This suggests that morphological relationships identified at conventional block scales cannot be transferred directly to activity-derived clusters without considering spatial extent and organizational scale.

5.3. Potential Planning Implications for Urban Regeneration

Based on the observed cluster profiles and micro-scale characteristics, this study outlines a potential application pathway linking cluster identification, morphological diagnosis, type profiling, and planning translation. At the network level, multi-core chains, main-axis corridors, continuous commercial frontages, and public-transport nodes can serve as diagnostic references for identifying discontinuities in spatial organization and accessibility.

At the type level, the results suggest differentiated potential priorities. High-density large-area clusters may warrant attention to public-space pressure, branch-road continuity, and multi-core linkage; High-density small-area clusters to pocket spaces, short-segment stitching, and multi-axis connections; Medium-density large-area clusters to main-axis continuity and lateral street-front activation; Medium-density small-area clusters to strengthening existing linear street structures; and Low-density small-area clusters to basic-service provision, slow-mobility connectivity, and local-node cultivation. Vitality clusters therefore do not replace existing planning-control units, but provide an activity-based diagnostic reference for identifying regeneration areas, calibrating boundaries, and delineating strategy zones. For clusters extending across administrative jurisdictions, this diagnostic layer is intended to support cross-boundary problem identification and coordination, whereas specific interventions would still need to be translated into and implemented through existing statutory planning and administrative units.

5.4. Implications for Urban Environmental Big-Data Analytics

Recent urban big-data and GeoAI research has substantially improved the sensing, prediction, and explanation of urban spatial conditions [50,51]. The contribution of the present study lies not in introducing another predictive model, but in shifting the analytical object from vitality values attached to predefined spatial units toward activity-derived clusters that can subsequently be interpreted across cluster and micro scales. This extends big-data vitality analysis from identifying where activity is concentrated toward examining how such concentrations are spatially organized and how they may inform regeneration diagnosis. In this sense, the methodological contribution is the linkage between data-driven spatial-unit construction and multi-scale morphological interpretation rather than the upstream identification algorithm itself.

5.5. Limitations and Future Research

This study has several limitations. First, the analysis is based on the Nanjing Metropolitan Area, and the identified patterns and operational thresholds may not be directly transferable to other metropolitan contexts. The results may also be sensitive to the 500 m UIB analytical scale and the associated modifiable areal unit problem (MAUP), and the cluster boundaries should not be interpreted as a unique ground-truth delineation of urban activity space. Future research could test transferability and bound-

ary stability across metropolitan contexts and alternative analytical scales.

Second, the analysis is primarily cross-sectional, and the activity observations and contextual spatial datasets are not fully synchronous. The study therefore does not capture the temporal evolution or persistence of vitality-cluster boundaries. Future research should employ temporally aligned multi-period mobility and contextual datasets to examine the stability and evolution of these spatial patterns.

Third, although the revised statistical analysis incorporates FDR correction, robustness testing, and global Moran's I diagnostics, local spatial dependence and sensitivity to alternative spatial-weight specifications cannot be fully excluded. Larger cluster samples and spatially explicit inferential models could further strengthen the statistical assessment.

Fourth, the planning translation and micro-scale interpretation are still based mainly on indicator analysis and purposively selected representative cases rather than on implemented regeneration projects or independent external validation. Future work could incorporate actual planning-control units, post-implementation evaluation, pedestrian or mobility observations, and a broader set of cases to further assess the practical applicability and fine-scale interpretability of vitality clusters.

6. Conclusions

First, the 34 vitality clusters exhibit interpretable spatial relationships with administrative units and built-up territories while also showing cross-boundary spatial continuity in several cases. Their area and population distributions display distinct rank–size patterns relative to administrative units and built-up territories. Together, these comparisons support the interpretation of vitality clusters as activity-informed analytical units with identifiable spatial correspondence and cross-boundary continuity.

Second, vitality clusters in the Nanjing Metropolitan Area exhibit clear operational area–density grouping patterns and spatial gradients. Most clusters are concentrated within 50–100 km^2 and 2000–3000 persons/km^2, showing the dominant characteristics of medium density and small scale. Large clusters such as #189 and #130 exhibit cross-administrative boundaries, multi-core organization, and regional radiation, indicating that actual urban vitality space does not fully conform to administrative boundaries and instead exhibits cross-boundary continuity associated with activity concentration, functional linkages, and contiguous urbanized space.

Third, vitality clusters differ significantly in road structure, geometric form, distribution and agglomeration, accessibility and connectivity, and functional structure. High vitality does not necessarily correspond to high compactness. Super-large metropolitan core clusters often have low compactness, high boundary complexity, and broad functional distribution, whereas medium- and small-city clusters may show higher compactness, stronger core functional agglomeration, and greater road-network density.

Fourth, the revised inter-group analysis identifies systematic differences among the operationally defined cluster groups. After controlling for multiple testing, 30 of 60 non-redundant variables remain significant, with differences concentrated mainly in functional, transport, and morphological characteristics. An all-Kruskal–Wallis robustness analysis retains 25 variables, all of which belong to the primary significant set. These results provide evidence of multidimensional inter-group differentiation, although they should not be interpreted as independent statistical validation of the typology.

Fifth, micro-scale case examination illustrates how cluster-level morphological differences can be expressed in block grain, street interfaces, local functional organization, and walking conditions. Across the selected representative cases, small blocks, continuous ground-floor interfaces, local mixed uses, and favorable walking conditions tend to

co-occur, providing case-based support for the finer-scale interpretability of vitality clusters.

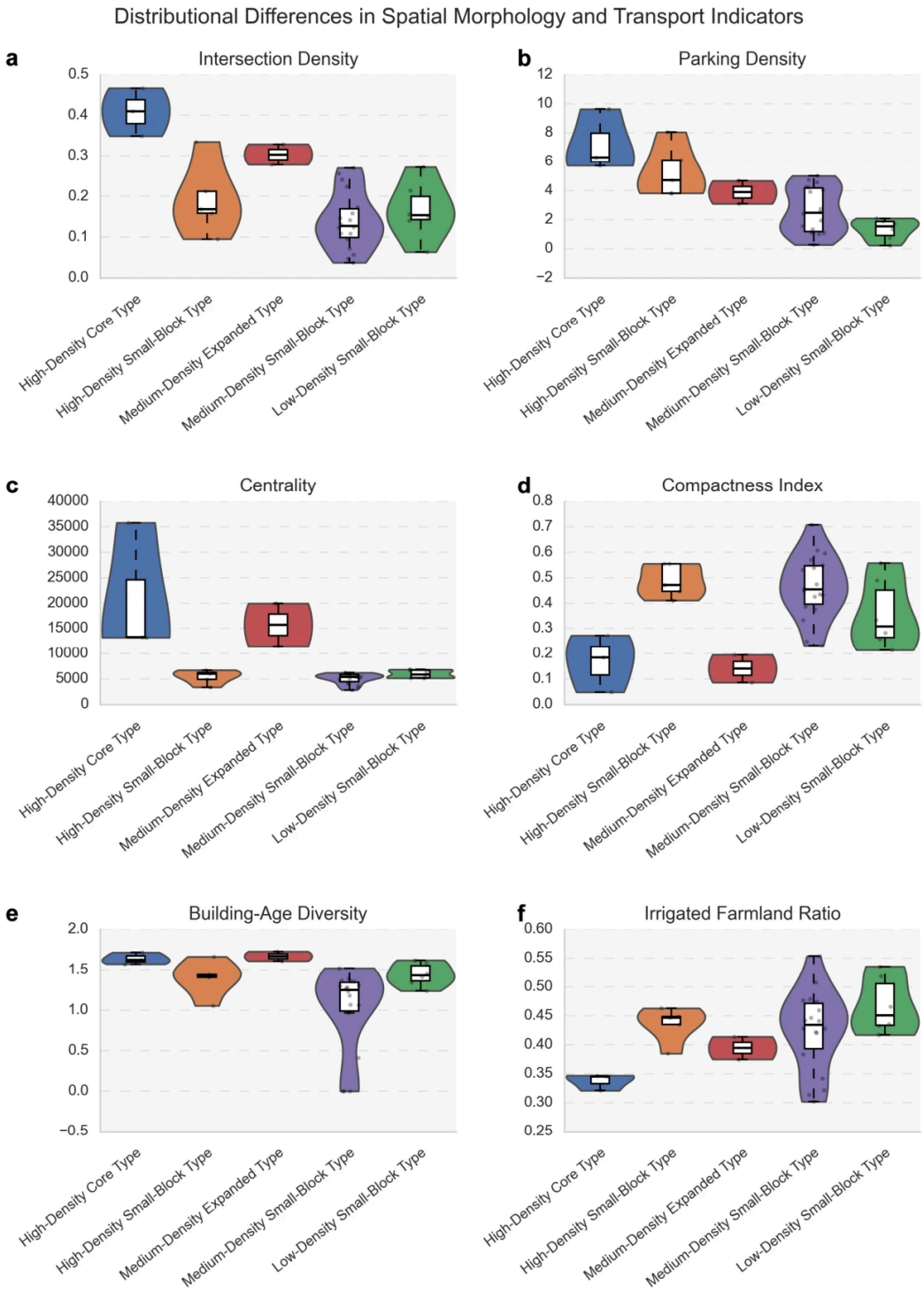


Figure 10. Distributional differences in spatial-morphology and transport indicators across the operational vitality-cluster groups. (a) Intersection density; (b) parking density; (c) centrality; (d) compactness index; (e) building-age diversity; (f) irrigated-farmland ratio. Violin plots show the distribution of each indicator within the five operational area–density groups, while the embedded boxplots indicate the median and interquartile range and the individual points represent observed cluster values.

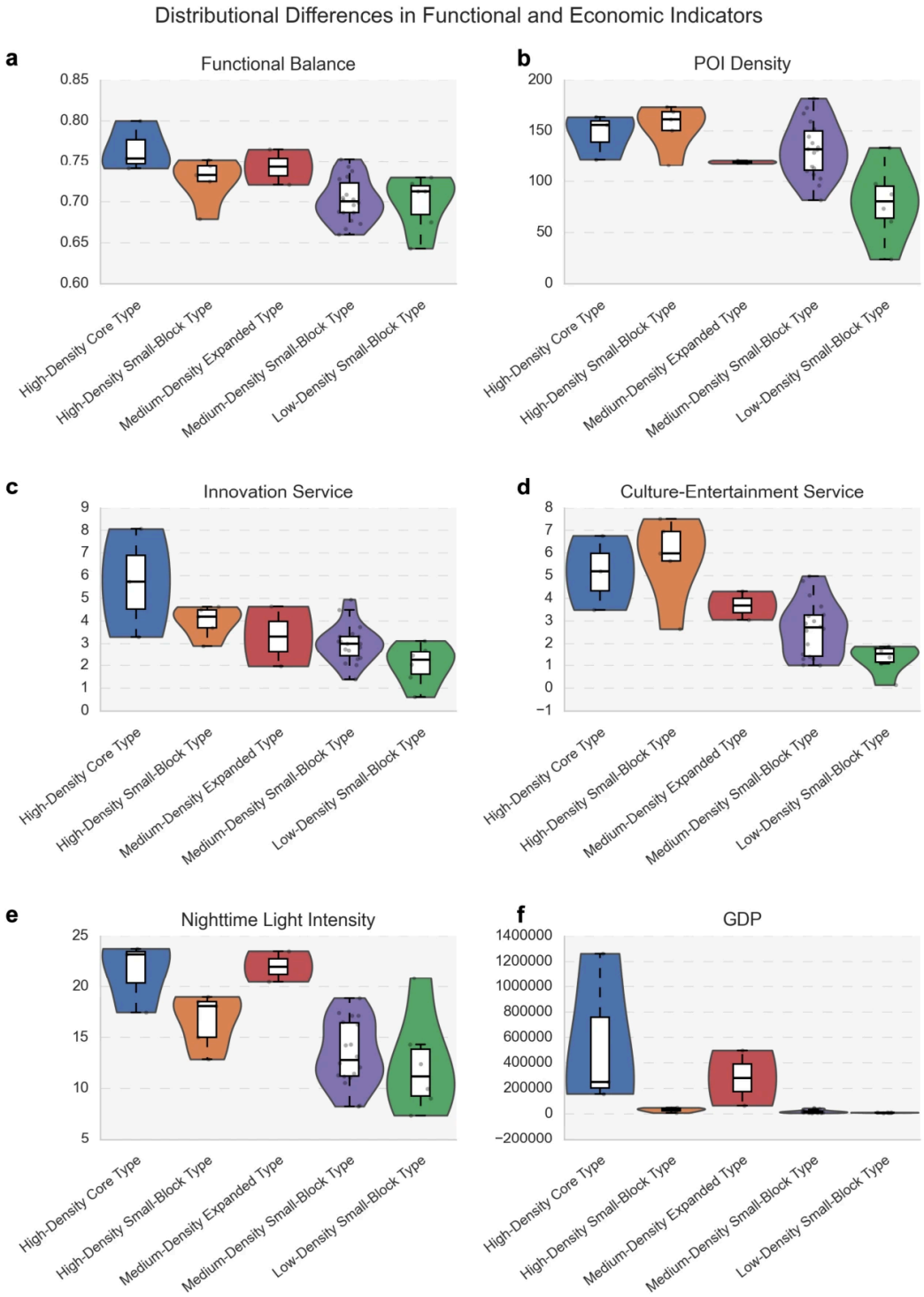


Figure 11. Distributional differences in functional and economic indicators across the operational vitality-cluster groups. (a) Functional balance; (b) POI density; (c) innovation-service level; (d) culture–entertainment service level; (e) nighttime-light intensity; (f) GDP. Violin plots show the within-group distributions, embedded boxplots indicate the median and interquartile range, and individual points represent observed cluster values.

Supplementary Materials: The following supporting information can be downloaded at: https://www.mdpi.com/article/doi/s1, Figure S1: title; Table S1: title; Video S1: title.

Author Contributions: Conceptualization, Zhenyu Wang and Fengliang Tang; methodology, Zhenyu Wang; software, Zhenyu Wang, Yunfa Wu and Weixing Xu; validation, Zhenyu Wang, Yunfa Wu, Fengliang Tang and Weixing Xu; formal analysis, Zhenyu Wang and Weixing Xu; inves-

tigation, Zhenyu Wang, Yunfa Wu and Fengliang Tang; resources, Yunfa Wu; data curation, Zhenyu Wang, Yunfa Wu and Weixing Xu; writing—original draft preparation, Zhenyu Wang and Yunfa Wu; writing—review and editing, Zhenyu Wang and Weixing Xu; visualization, Zhenyu Wang, Yunfa Wu and Weixing Xu; supervision, Zhenyu Wang, Yunfa Wu and Weixing Xu; project administration, Fengliang Tang; funding acquisition, Fengliang Tang and Weixing Xu. All authors have read and agreed to the published version of the manuscript.

Funding: This work was supported by the National Natural Science Foundation of China (52478001).

Data Availability Statement: The data supporting the reported results are available upon reasonable request to the first author.

Conflicts of Interest: The authors declare no conflicts of interest.

References

1. Long, Y.; Huang, C.C. Does Block Size Matter? The Impact of Urban Design on Economic Vitality for Chinese Cities. *Environ. Plan. B Urban Anal. City Sci.* **2017**, *46*, 406–422. [Google Scholar] [CrossRef]
2. Hasanzadeh, K.; Purkarthofer, E.; Kajosaari, A.; Kyttä, M. Redefining Neighborhood Boundaries Using Activity Spaces: Bringing Together Soft Spaces and Spatial Analysis to Further the Discussion on Planning in Functional Spaces. *J. Plan. Educ. Res.* **2025**, *45*, 878–890. [Google Scholar] [CrossRef]
3. Jin, M.; Gong, L.; Cao, Y.; Zhang, P.; Gong, Y.; Liu, Y. Identifying Borders of Activity Spaces and Quantifying Border Effects on Intra-Urban Travel through Spatial Interaction Network. *Comput. Environ. Urban Syst.* **2021**, *87*, 101625. [Google Scholar] [CrossRef]
4. Kwan, M.-P. The Uncertain Geographic Context Problem. *Ann. Assoc. Am. Geogr.* **2012**, *102*, 958–968. [Google Scholar] [CrossRef]
5. Wong, D.W.S. The Modifiable Areal Unit Problem (MAUP). In *WorldMinds: Geographical Perspectives on 100 Problems*; Janelle, D.G., Warf, B., Hansen, K., Eds.; Springer Netherlands: Dordrecht, The Netherlands, 2004; pp. 571–575. [Google Scholar]
6. Huang, H.; Yao, X.A.; Krisp, J.M.; Jiang, B. Analytics of Location-Based Big Data for Smart Cities: Opportunities, Challenges, and Future Directions. *Comput. Environ. Urban Syst.* **2021**, *90*, 101712. [Google Scholar] [CrossRef]
7. Yang, Y.; Wang, H.; Qin, S.; Li, X.; Zhu, Y.; Wang, Y. Analysis of Urban Vitality in Nanjing Based on a Plot Boundary-Based Neural Network Weighted Regression Model. *ISPRS Int. J. Geo-Inf.* **2022**, *11*, 624. [Google Scholar] [CrossRef]
8. Chen, Y.; Yu, B.; Shu, B.; Yang, L.; Wang, R. Exploring the Spatiotemporal Patterns and Correlates of Urban Vitality: Temporal and Spatial Heterogeneity. *Sustain. Cities Soc.* **2023**, *91*, 104440. [Google Scholar] [CrossRef]
9. Ye, Y.; Li, D.; Liu, X. How Block Density and Typology Affect Urban Vitality: An Exploratory Analysis in Shenzhen, China. *Urban Geogr.* **2017**, *39*, 631–652. [Google Scholar] [CrossRef]
10. Tang, S.; Ta, N. How the Built Environment Affects the Spatiotemporal Pattern of Urban Vitality: A Comparison among Different Urban Functional Areas. *Comput. Urban Sci.* **2022**, *2*, 39. [Google Scholar] [CrossRef] [PubMed]
11. Li, Q.; Cui, C.; Liu, F.; Wu, Q.; Run, Y.; Han, Z. Multidimensional Urban Vitality on Streets: Spatial Patterns and Influence Factor Identification Using Multisource Urban Data. *ISPRS Int. J. Geo-Inf.* **2021**, *11*, 2. [Google Scholar] [CrossRef]
12. Wang, Z.; Xia, N.; Zhao, X.; Gao, X.; Zhuang, S.; Li, M. Evaluating Urban Vitality of Street Blocks Based on Multi-Source Geographic Big Data: A Case Study of Shenzhen. *Int. J. Environ. Res. Public Health* **2023**, *20*, 3821. [Google Scholar] [CrossRef] [PubMed]
13. Li, X.; Li, Y.; Jia, T.; Zhou, L.; Hijazi, I.H. The Six Dimensions of Built Environment on Urban Vitality: Fusion Evidence from Multi-Source Data. *Cities* **2022**, *121*, 103482. [Google Scholar] [CrossRef]
14. Wang, Z.; Wang, X.; Liu, Y.; Zhu, L. Identification of 71 Factors Influencing Urban Vitality and Examination of Their Spatial Dependence: A Comprehensive Validation Applying Multiple Machine-Learning Models. *Sustain. Cities Soc.* **2024**, *108*, 105491. [Google Scholar] [CrossRef]
15. Yin, J.; Soliman, A.; Yin, D.; Wang, S. Depicting Urban Boundaries from a Mobility Network of Spatial Interactions: A Case Study of Great Britain with Geo-Located Twitter Data. *Int. J. Geogr. Inf. Sci.* **2017**, *31*, 1293–1313. [Google Scholar] [CrossRef]
16. Yuan, J.; Zheng, Y.; Xie, X. Discovering Regions of Different Functions in a City Using Human Mobility and POIs. In *Proceedings of the 18th ACM SIGKDD International Conference on Knowledge Discovery and Data Mining*; Association for

Computing Machinery: New York, NY, USA, 2012; pp. 186–194. [Google Scholar]
17. Jiang, D. *The Theory of City Form Vitality*; Southeast University Press: Nanjing, China, 2007. [Google Scholar]
18. Wang, M.; Vermeulen, F. Life between Buildings from a Street View Image: What Do Big Data Analytics Reveal about Neighbourhood Organisational Vitality? *Urban Stud.* **2020**, *58*, 3118–3139. [Google Scholar] [CrossRef]
19. Carlucci, M.; Zambon, I.; Salvati, L. Diversification in Urban Functions as a Measure of Metropolitan Complexity. *Environ. Plan. B Urban Anal. City Sci.* **2020**, *47*, 1289–1305. [Google Scholar] [CrossRef]
20. Zeng, P.; Wei, M.; Liu, X. Investigating the Spatiotemporal Dynamics of Urban Vitality Using Bicycle-Sharing Data. *Sustainability* **2020**, *12*, 1714. [Google Scholar] [CrossRef]
21. Jacobs, J. *The Death and Life of Great American Cities*; Random House: New York, NY, USA, 1961. [Google Scholar]
22. Gehl, J. *Livet Mellem Husene*; Arkitektens Forlag: Copenhagen K, Denmark, 2003. [Google Scholar]
23. Montgomery, J. Making a City: Urbanity, Vitality and Urban Design. *J. Urban Des.* **2007**, *3*, 93–116. [Google Scholar] [CrossRef]
24. Wei, Z.; Mukherjee, S. Examining Income Segregation within Activity Spaces under Natural Disaster Using Dynamic Mobility Network. *Sustain. Cities Soc.* **2023**, *91*, 104408. [Google Scholar] [CrossRef]
25. Liu, S.; Zhang, L.; Long, Y.; Long, Y.; Xu, M. A New Urban Vitality Analysis and Evaluation Framework Based on Human Activity Modeling Using Multi-Source Big Data. *ISPRS Int. J. Geo-Inf.* **2020**, *9*, 617. [Google Scholar] [CrossRef]
26. Liu, L.; Silva, E.A.; Wu, C.; Wang, H. A Machine Learning-Based Method for the Large-Scale Evaluation of the Qualities of the Urban Environment. *Comput. Environ. Urban Syst.* **2017**, *65*, 113–125. [Google Scholar] [CrossRef]
27. Mouratidis, K.; Poortinga, W. Built Environment, Urban Vitality and Social Cohesion: Do Vibrant Neighborhoods Foster Strong Communities? *Landsc. Urban Plan.* **2020**, *204*, 103951. [Google Scholar] [CrossRef]
28. Wu, C.; Ye, Y.; Gao, F.; Ye, X. Using Street View Images to Examine the Association between Human Perceptions of Locale and Urban Vitality in Shenzhen, China. *Sustain. Cities Soc.* **2023**, *88*, 104291. [Google Scholar] [CrossRef]
29. Fotheringham, A.S.; Wong, D.W.S. The Modifiable Areal Unit Problem in Multivariate Statistical Analysis. *Environ. Plan. A Econ. Space* **1991**, *23*, 1025–1044. [Google Scholar] [CrossRef]
30. Fang, C.; Zhou, L.; Gu, X.; Liu, X.; Werner, M. A Data Driven Approach to Urban Area Delineation Using Multi Source Geospatial Data. *Sci. Rep.* **2025**, *15*, 8708. [Google Scholar] [CrossRef] [PubMed]
31. Pang, M.; Binder, C.R.; Golay, F. An Empirical Comparative Analysis of Functional and Perceived Neighbourhood Boundaries across Geneva, Switzerland. *Cities* **2024**, *146*, 104786. [Google Scholar] [CrossRef]
32. Cagney, K.A.; Cornwell, E.Y.; Goldman, A.W.; Cai, L. Urban Mobility and Activity Space. *Annu. Rev. Sociol.* **2020**, *46*, 623–648. [Google Scholar] [CrossRef]
33. Qian, Z.; Liu, X.; Tao, F.; Zhou, T. Identification of Urban Functional Areas by Coupling Satellite Images and Taxi GPS Trajectories. *Remote Sens.* **2020**, *12*, 2449. [Google Scholar] [CrossRef]
34. Xie, Y.; Fu, X.; Long, Y.; Pei, M. Identifying Urban Functional Regions: A Multi-Dimensional Framework Approach Integrating Metro Smart Card Data and Car-Hailing Data. *Environ. Plan. B Urban Anal. City Sci.* **2025**, *52*, 614–628. [Google Scholar] [CrossRef]
35. Zheng, H.; He, B.; Liu, Y.; Li, X. Deconstruction of Commuters' Activity Space and Social Exclusion under Anchor Point Theory: A Case Study of Kunming, China. *Transp. Res. Rec.* **2023**, *2677*, 1481–1495. [Google Scholar] [CrossRef]
36. Di, H.; Gong, S.; Wang, C.; Zhu, W.; Jing, C. Profiling Urban Functional Regions with POI and Wi-Fi Data: A Dual-Entropy Approach and Demographic Analysis. *Trans. GIS* **2026**, *30*, e70330. [Google Scholar] [CrossRef]
37. Carmona, M. *Public Places Urban Spaces: The Dimensions of Urban Design*, 3rd ed.; Routledge: New York, NY, USA, 2021. [Google Scholar]
38. Yang, L.; Wu, M.; Chen, Y.; Wu, C. Examining the Impact of the Urban Transportation System on Tangible and Intangible Vitality at the City-Block Scale in Nanjing, China. *Environ. Plan. B Urban Anal. City Sci.* **2024**, *51*, 1833–1853. [Google Scholar] [CrossRef]
39. Kickert, C.C. Active Centers—Interactive Edges: The Rise and Fall of Ground Floor Frontages. *URBAN DES. Int.* **2016**, *21*, 55–77. [Google Scholar] [CrossRef]
40. Wangbao, L. Spatial Impact of the Built Environment on Street Vitality: A Case Study of the Tianhe District, Guangzhou. *Front. Environ. Sci.* **2022**, *10*, 966562. [Google Scholar] [CrossRef]
41. Wang, Y.; Niu, X. Polycentricity Measurement of China's Urban Agglomerations Considering Internal and External Connections. *Front. Urban Rural Plan.* **2023**, *1*, 19. [Google Scholar] [CrossRef]

42. Wang, Z.; Xu, W.; Liu, Y.; Liu, B.; Zhu, L. Urban Vitality Transfer: Analysis of 50 Factors Based on 24-h Weekday Activity in Nanjing. *Front. Archit. Res.* **2025**, *14*, 1249–1273. [Google Scholar] [CrossRef]
43. Gurski, C.J.; Dittel, B.N. Making Multiple Comparisons Easy: A Decision Tree and Visual Statistics Guide for Data with More than Two Groups. *ImmunoHorizons* **2026**, *10*, vlaf072. [Google Scholar] [CrossRef] [PubMed]
44. Mondal, H.; Mondal, S.; Majumder, R.; De, R. Conduct Common Statistical Tests Online. *Indian Dermatol. Online J.* **2022**, *13*, 539. [Google Scholar] [CrossRef] [PubMed]
45. Score, W. *Walk Score Methodology*; Walk Score: Seattle, WA, USA, 2014. [Google Scholar]
46. Zhang, B.; Zhong, C.; Gao, Q.; Shabrina, Z.; Tu, W. Delineating Urban Functional Zones Using Mobile Phone Data: A Case Study of Cross-Boundary Integration in Shenzhen-Dongguan-Huizhou Area. *Comput. Environ. Urban Syst.* **2022**, *98*, 101872. [Google Scholar] [CrossRef]
47. Cao, W.; Dong, L.; Cheng, Y.; Wu, L.; Guo, Q.; Liu, Y. Constructing Multi-Level Urban Clusters Based on Population Distributions and Interactions. *Comput. Environ. Urban Syst.* **2023**, *99*, 101897. [Google Scholar] [CrossRef]
48. Chen, W.; Wu, A.N.; Biljecki, F. Classification of Urban Morphology with Deep Learning: Application on Urban Vitality. *Comput. Environ. Urban Syst.* **2021**, *90*, 101706. [Google Scholar] [CrossRef]
49. Zhang, A.; Li, W.; Wu, J.; Lin, J.; Chu, J.; Xia, C. How Can the Urban Landscape Affect Urban Vitality at the Street Block Level? A Case Study of 15 Metropolises in China. *Environ. Plan. B Urban Anal. City Sci.* **2021**, *48*, 1245–1262. [Google Scholar] [CrossRef]
50. Kong, L.; Liu, Z.; Wu, J. A Systematic Review of Big Data-Based Urban Sustainability Research: State-of-the-Science and Future Directions. *J. Clean. Prod.* **2020**, *273*, 123142. [Google Scholar] [CrossRef]
51. Liu, P.; Biljecki, F. A Review of Spatially-Explicit GeoAI Applications in Urban Geography. *Int. J. Appl. Earth Obs. Geoinf.* **2022**, *112*, 102936. [Google Scholar] [CrossRef]

Disclaimer/Publisher's Note: The statements, opinions and data contained in all publications are solely those of the individual author(s) and contributor(s) and not of MDPI and/or the editor(s). MDPI and/or the editor(s) disclaim responsibility for any injury to people or property resulting from any ideas, methods, instructions or products referred to in the content.